

**Applying Radar Cross-Section Estimations to Minimize Radar Echo  
in Unmanned Combat Air Vehicle Design**

Jillian G. Yuricich

2016

Thesis Committee:

Dr. Clifford Whitfield, Advisor

Dr. Richard Freuler

Department of Mechanical and Aerospace Engineering

Presented in Partial Fulfillment of the Requirements for Graduation with Honors Research  
Distinction in Aeronautical and Astronautical Engineering at The Ohio State University

## Abstract

Radar profoundly altered the development of vehicle technology for combat especially in the realm of aircraft design. The technique of purpose-shaping an aircraft to minimize the vehicle's radar cross-section and avoid detection on radar systems became a crucial step in the development of conceptual air vehicles, however much of this work is classified by the U.S. government. The purpose of this research is to develop the best methodology for predicting the radar cross-section of an aircraft throughout the design process by using open source radar equations. In order to estimate a radar cross-section value, simple shapes and their known radar cross-section expressions were used to represent all features of the conceptual aircraft design. An unmanned combat air vehicle designated the QF-36 Thunder was designed specifically for a radar-cross section analysis. Each of the QF-36's main components, including wings, tails, and fuselage shape, were analyzed and their radar-cross section contribution calculated to ascertain the overall aircraft radar cross-section. Adjustments to specific aspects of the QF-36 could then be made to minimize the overall radar cross-section value while maintaining performance specifications set by the Request for Proposal which defined the vehicle's mission. Following the development of this radar-cross section estimation tool, the results showed that large volume components including the fuselage and wing contributed the most to the total radar-cross section especially in the side- and front-view respectively. This trend aligns well with the initial idea of which aspects would contribute most to the radar-cross section. However, the main design advantage found throughout this process was that the tails contribute much less to the overall radar-cross section than initially hypothesized. This allows for large tails and better maneuverability with little increase in the overall radar echo. With this observation, design strategies may focus on minimizing wing size and maximizing tail size for the best compromise between radar-cross section minimization and enhanced performance. This research reflects one of few studies that documents the methodology for estimating radar cross-section of an aircraft in its entirety.

## Acknowledgements

First, I would like to dedicate this work to my parents and my sister without whom I would be lost. I also want to thank Dr. Clifford Whitfield for his guidance, encouragement, and general kindness throughout my time at Ohio State. He is a wonderful professor and person, and I am a better engineer because of him. I would also like to recognize the impression that Dr. Richard Freuler left on my life. He was the first professor I met at Ohio State, and our first meeting forever changed my college career. His mentorship has been one of the most valuable relationships I have made throughout my undergraduate experience. Finally, I would be remiss if I did not mention the wonderful friends I have made throughout my time at Ohio State in my Aeronautical and Astronautical Engineering courses. From late night study sessions around the dining room table to hours in the computer laboratory, we have been through so much together. I would not want to do it over again, but looking back, I would not change a thing. I love you all.

## Table of Contents

Abstract .....	ii
Acknowledgements .....	iii
Table of Contents .....	iv
List of Figures .....	v
List of Tables .....	vi
Nomenclature .....	vii
1. Introduction .....	1
1.1 The Radar Equation .....	2
1.2 General Purpose-Shaping Knowledge .....	4
2. Characteristic Wavelength Determination .....	7
3. UCAV Development and Design .....	13
3.1 Project Needs and Specifications Screening .....	13
3.2 Air Vehicle Configuration Options .....	15
3.3 Final Configuration Selection .....	19
3.4 QF-36 Concept .....	22
4. Radar-Cross Section Calculations .....	23
4.1 UCAV Profile Selection .....	23
4.2 Front-View RCS Estimation .....	23
4.3 Side-View RCS Estimation .....	32
5. Discussion and Design Implications .....	36
6. Conclusion .....	42
References .....	44
Appendix A: AIAA Request for Proposal .....	1
Appendix B: QF-36 Concept Design Drawings .....	1
Appendix C: Additional Information .....	<b>Error! Bookmark not defined.</b>

## List of Figures

Figure 1: F-117A planform and faceted nose with radar reflection representation.....	5
Figure 2: F-22 in formation flight with radar signal reflection.....	6
Figure 3: Diagram of cylinders used to model a 95th-percentile male.....	10
Figure 4: UCAV screening chart. ....	14
Figure 5: Tailless aircraft with control-canard surface. ....	15
Figure 6: The B-2 bomber aircraft, an example of a tailless configuration. ....	16
Figure 7: Example of a tailless aircraft. ....	17
Figure 8: Delta wing configuration (A) and cranked arrow wing configuration (B).....	18
Figure 9: Conventional aircraft layout of the F-22 Raptor. ....	18
Figure 10: UCAV scoring chart.....	21
Figure 11: QF-36 Thunder concept.....	22
Figure 12: Front-view of UCAV.....	23
Figure 13: Ogive and fuselage profile comparison with varying radii. ....	25
Figure 14: Ogive and fuselage cross-section comparison with varying radii.....	26
Figure 15: Ogive coordinate system and labels for side-view RCS estimation.....	27
Figure 16: Side-view of UCAV .....	33
Figure 17: Flat plate RCS estimation with tail and wing front-view examples.....	38

## List of Tables

Table 1: Radar cross-section estimations for various shapes at $\theta = 0^\circ$ [4]. .....	3
Table 2: RCS values for various vehicles and objects. ....	7
Table 3: Anthropomorphic dimensions for 95 <sup>th</sup> -percentile American male [12, 13]. ....	9
Table 4: RCS distribution for each component of the 95 <sup>th</sup> -percentile male figure. ....	9
Table 5: UCAV design criteria and requirements as set by AIAA RFP. ....	13
Table 6: Front-view estimated values for forward fuselage. ....	28
Table 7: Front-view estimated values for tail surfaces. ....	29
Table 8: Front-view estimated values for wing surfaces. ....	30
Table 9: Front-view estimated values for the wing. ....	31
Table 10: Front-view estimated values for the engine nacelles. ....	32
Table 11: Total RCS of the QF-36 in the front-view. ....	32
Table 12: Side-view estimated values for the tail. ....	33
Table 13: Fuselage represented by multiple spindles in the side view. ....	34
Table 14: Total RCS for the QF-36 in the side-view. ....	35
Table 15: Various RCS estimations for past and present military aircraft and QF-36 concept. ....	36

## Nomenclature

AIAA	American Institute of Aeronautics and Astronautics
FLA	Forward Looking Aft
GHz	Gigahertz (unit of electromagnetic wave equal to one billion hertz)
HF	High Frequency radar
JSF	Joint Strike Fighter (reference to the F-35 program)
MEADS	Medium Extended Air Defense System (radar system constructed by the United States, Italy, and Germany)
MHz	Megahertz (unit of electromagnetic wave equal to one million hertz)
OTH	Over The Horizon radar system
RFP	Request for Proposal
RCS	Radar Cross-Section
UCAV	Unmanned Combat Aerial Vehicle
UHF	Ultra-High Frequency radar
VHF	Very High Frequency radar

## 1. Introduction

The use of radar in combat settings dramatically altered the course of vehicle technology in the 20<sup>th</sup> century. Introduced in World War II as a means of tracking enemy tanks, ships, and planes, radar became an important investment for militaries globally. Radar operates by emitting radio waves, or signals, delivered from a transmitter. If the radar signal contacts an object, the waves are reflected back to a receiver. Using the speed of the waves and the time delay between transmission and reception, the object's distance from the radar source can be calculated. The magnitude of the signal on the return transmission is also proportional to the size of the object detected. A larger object has a larger radar echo, also known as and henceforth referred to as radar cross-section (RCS) [1].

Radar was not without competition, however, and was countered with developments in stealth, or low-observable, technologies. Within the last few decades, stealth characteristics have advanced into one of the most critical aspects of military combat aircraft design [2]. These technologies aim to increase air vehicle survivability by reducing the radar cross-section. While many technologies such as radar-absorbing paint are included during the late stages of an air vehicle's development to reduce RCS, purpose-shaping is a method that can be applied from the inception of a new aircraft design. Purpose-shaping techniques reduce the RCS by designing the geometry of the air vehicle's surface with the intention of reflecting radar waves away from the radar signal receiver [3].

This research investigated the use of equations for radar reflection and mathematical estimations of simple shapes' RCS values to determine a method for estimating the RCS of an air vehicle at a single stage of the design process. This would allow the designer to better understand which



aspects of the vehicle design contribute the most toward the RCS in a quick, low-fidelity manner as the design is manipulated to meet other performance parameters. The aircraft to be used in this analysis is a design for an Unmanned Combat Aerial Vehicle (UCAV). The UCAV class of aircraft will play a crucial role in the future of military aviation. With the current use of drone technology in military reconnaissance, there will come a time where aviation technology in the military matures enough for unmanned systems to be used in a fighter-combat role. This trend was seen throughout World War I where once only used in reconnaissance missions, the maturation of airplanes led to their use in combat in World War II opening up a new frontier of aviation. This analysis of the UCAV is therefore very relevant to modern design studies.

## 1.1 The Radar Equation

Because existing approaches for calculating an aircraft's exact RCS signature and size are classified by the United States Department of Defense, this research will demonstrate the ability to use open source equations to estimate an aircraft's RCS value for use in conceptual design. It was first necessary to understand the mathematical basis for radar and how it functions. The fundamentals of radar can be observed within the radar equation which has been manipulated to solve for range ( $R$ ):

$$R = \left( \frac{P_t G_t G_r \sigma \lambda^2}{(4\pi)^3 P_r} \right)^{1/4} \quad (1)$$

where  $P_t$  and  $P_r$  (watts) are the transmitted power from the radar transmitter and receiver, respectfully,  $G_t$  and  $G_r$  (unitless) are the gains of the transmitter and receiver,  $\sigma$  (square meters) is the RCS and  $\lambda$  (meters) is the wavelength which can be calculated by:

$$\lambda = \frac{c}{f} \quad (2)$$

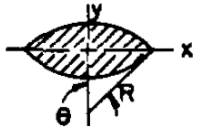
where  $c$ , the speed of light, equals  $3 \times 10^8$  (meters per second) and  $f$  is the radiated signal's frequency (Hertz). Since the  $\sigma$  (RCS) value only varies by the fourth root, only large changes in RCS value will contribute to narrowing the range in which the aircraft would be detected [3]. However, once in range, any amount of RCS reduction will help evade enemy detection.

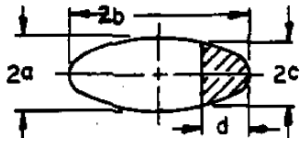
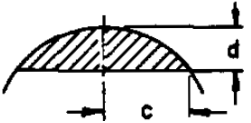
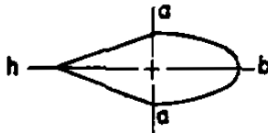
With the RCS identified in the range equation, it was then important to understand how to quantify a three-dimensional shape's radar echo mathematically. These were the most useful equations for this research. The main source of these RCS equations for simple shapes was a paper by Crispin and Maffett [4]. This paper outlined the RCS calculations for generic spheroid shapes at various angles of radar signal impingement. Spheroid have an RCS ( $\sigma$ ) of:

$$\sigma = \frac{4}{\pi} k^4 V^2 \left[ 1 + \frac{1}{\pi y} e^{-y} \right]^2 \quad (3)$$

where  $y = b/a$ ,  $V$  is volume, and  $k = 2\pi/\lambda$  where  $\lambda$  is the wavelength of the emitted radar signal [4]. Manipulating this for specific spheroid shapes, the table below gives examples of equations used to calculate the RCS ( $\sigma$ ) given the shape's geometric values. These equations are only valid at a signal impingement angle of zero-degrees.

**Table 1: Radar cross-section estimations for various shapes at  $\theta = 0^\circ$  [4].**

Shape	Geometry	RCS Expression
Lens (revolved around y-axis)		$y = \frac{3V}{4\pi R^3 \sin^3 \theta}$ $V = \frac{2\pi R^3}{3} (1 - \cos \theta)(1 - \cos \theta + \sin^2 \theta)$

Elliptic Ogive		$y = \frac{3V}{4\pi b^3(1 - \cos \theta)^3}$ $V = 2\pi ab^2(\sin \theta - \theta \cos \theta - \frac{1}{3}\sin^3 \theta)$
Spindle (Paraboloid Ogive)		$y = \frac{4c}{5d}; V = \frac{16\pi cd^2}{15}$
Finite Cylinder	Length = h, base radius = a	$y = \frac{3h}{4a}; V = \pi a^2 h$
Cone-spheroid		$y = \frac{h + 2b}{4a}; V = \frac{\pi a^2(h + 2b)}{3}$

Further information on the topic provided RCS equations for varying angles of radar signal impingement for the spheroid as well as non-spheroid shapes including the cone, flat plate, and very thin cylinder, or wire. These equations will be discussed at length when used.

## 1.2 General Purpose-Shaping Knowledge

As aforementioned, exact RCS calculations and techniques of purpose-shaping are classified, but there is a wealth of general knowledge that exists regarding which shapes, surfaces, and aircraft features contribute to an air vehicle's RCS. A list of important features for designers to consider include large components such as the wing and tail surfaces and their edges, the engine compressor face, edges and flat sides to the air intakes, nozzle edges, and any 90-degree angles. It is also known that external fuel tanks, pods, and stores, the cockpit instrumentation, and pilot helmet contribute to a higher RCS. The UCAV already has an advantage here. Because this is an unmanned vehicle, there will be no cockpit in this design, and therefore no cockpit let alone instrumentation or helmet. However, other internal components on all aircraft give off their own

radar signals, including an altimeter, range seeker, GPS, and other avionic devices. Unfortunately, these will also contribute to an increased RCS [10].

Purpose shaping has three main approaches. The first is to use rectilinear and oblique surfaces much like the F-117A Nighthawk seen in the figure below. Developed in the 1970s, the basis for creating the initial design was based on a paper written by a Soviet mathematician in 1964. The paper was declassified by the Soviet government since the computer technology of the age could not make the part of the mathematical study a reality for designers. With this in the hands of American engineers at Skunk Works, the secret design group of the Lockheed Corporation, it was not long until the first stealth jet was born. Though very poor aerodynamically, these faceted faces cause the radar signals to scatter 99-percent of the radar signature energy. This was a massive leap in usable stealth technologies.



**Figure 1: F-117A planform and faceted nose with radar reflection representation.**

Another method is to shape the airframe such that the radar will reflect in a single direction. This strategy aims to have only one “sweet spot” where the aircraft’s RCS is at a high value, but the radar signal must come in from a very specific angle. At every other angle, the air vehicle would

be nearly undetectable. While this requires much coordination across all of the surfaces, it is very effective, as seen in the Figure 2 below [5]. The F-22 is an excellent example where surfaces are geometrically similar with parallel features and edges. The caveat of this design method is the single angle or narrow range of signal impingement angles of the radar where the RCS is astronomical on the aircraft. Fortunately, the F-22 has high performance capabilities and is maneuverable enough that should it be detected by luck, it would show up on radar only for a split second before disappearing again.

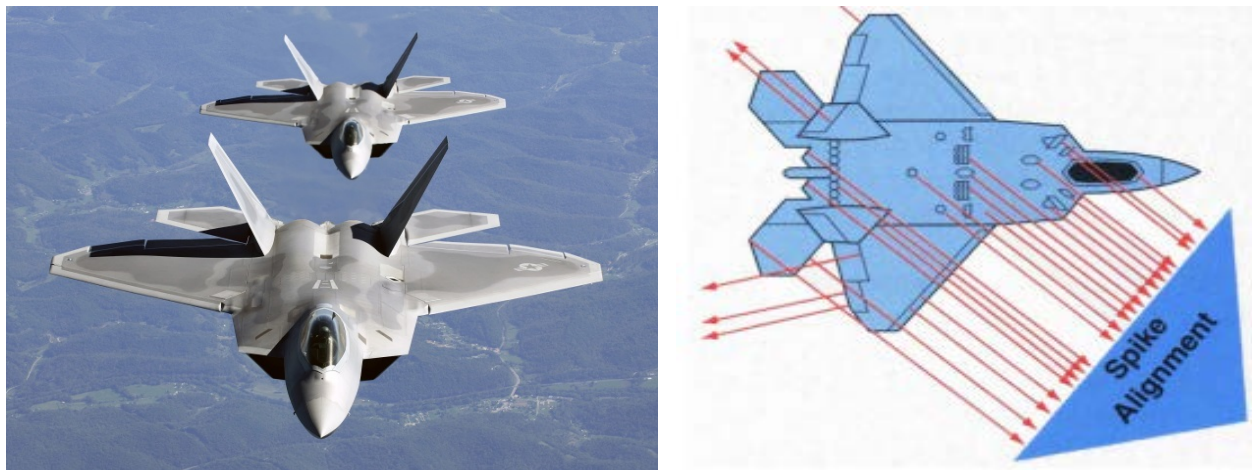


**Figure 2: F-22 in formation flight with radar signal reflection.**

The final purpose shaping method is to use blended external geometry with a continuously varying curvature. This shaping works because a constant curve reflects energy equally in all directions. This is especially useful when designing the internal components of air inlets [5].

In general, these techniques require much time and effort in order to produce a fully-developed aircraft with minimized RCS. Thus, while these techniques are understood, the application of each will be used in varying amounts throughout the design phase. Because the UCAV work will be a low-fidelity model, the varying application of these purpose-shaping options is sufficient.

## 2. Characteristic Wavelength Determination

A crucial part of this research was the investigation of what RCS values were reasonable for this subject matter. A table of information was discovered giving insight into various RCS values for a select group of vehicles and objects [10]. The table is provided below. While radar cross-section is usually given in square-meters, the RCS values have also been converted to square-feet since the UCAV design will be conducted in English units.

**Table 2: RCS values for various vehicles and objects.**

Object	RCS in M <sup>2</sup>	RCS in FT <sup>2</sup>
Medium to Large Bird	0.001	10.8(10 <sup>-4</sup> )
Conventional Winged Missile	0.1	1.076
Average Male	1	10.76
Small Fighter Jet	1	10.76
Helicopter	3	32.29
Larger Fighter Jet	6	64.58
Medium Jet Airliner	40	430.56
Automobile	100 - 200	1076 - 2152

As seen in Equation (3), the value  $k$  is necessary in order to calculate the RCS of the simple shape.

This value is defined as:

$$k = \frac{2\pi}{\lambda} \quad (4)$$

where  $\lambda$  is the wavelength of the radar system impinging on the aircraft's surface [4]. It was then necessary to estimate a reasonable wavelength value for the scenario.

Radio technologies operate on wavelengths ranging from tens to thousands of meters. For example, FM radio waves have a wavelength of four meters, whereas AM radio waves are roughly 500 meters to a kilometer long [8]. Radio waves for radar are in the range of one to ten meters. Lower-

frequency radar is very effective against stealth vehicles, and for radar frequencies less than 900 MHz, the RCS of the target vehicle increases exponentially regardless of any stealth geometry profile. This means that radar for use in detection and tracking, the system must strike a balance between a well-defined RCS signal and the ability to detect and differentiate between any object flying overhead. Low-frequency radar was used in Kosovo to track and shoot down the first stealth jet, the F-117 Nighthawk [9]. Currently, A- and B-band, or High Frequency (HF) and Very-High Frequency (VHF), radar systems range 300 MHz and below and have long been used as early warning and Over The Horizon (OTH) systems. However, these systems are limited by the size of their physical subsystems including antennas. Because of this limitation, C-Band, or Ultra-High Frequency (UHF), radar systems which range in operation from 300 MHz to 1 GHz are productive for detection and tracking of satellites and missiles over a long range especially for early warning and target acquisition missions [11]. An example of such a system is the Medium Extended Air Defense System (MEADS) which is an international program between the United States, German, and Italian militaries.

With this information, it was then possible to make an estimation of wavelength and check to see how reasonable the value is based on known information regarding radar systems. Because no declassified information exists on what radar frequencies or wavelengths are used in military radar systems, the human male example from Table 2 was used to determine a useful wavelength and, therefore, a  $k$  value. The profile of a human was replicated using the finite cylinder shape from Crispin and Maffett's paper as seen in Table 1. Cylinders of various dimensions represented the legs, torso with arms, and head of a 95<sup>th</sup>-percentile male. The 95<sup>th</sup>-percentile was chosen because a larger human would drive a higher RCS. Based on the equations from Crispin and Maffett, this

contributes to a lower wavelength necessary to achieve the intended RCS. A lower wavelength will in turn drive the aircraft RCS higher, which will overestimate the UCAV's RCS. Therefore, the RCS estimations are worst case scenario. The dimensions of the 95<sup>th</sup>-percentile male can be seen below.

**Table 3: Anthropomorphic dimensions for 95<sup>th</sup>-percentile American male [12, 13].**

<b>Feature</b>	<b>Dimension</b>
Bitragion Breadth (Head Width)	6.1 IN
Menton to top of head (Head Height)	9.1 IN
Head length (Head Depth)	8.2 IN
Shoulder (bideltoid) breadth (Torso Width)	21.1 IN
Mid-shoulder height, sitting (Torso Height)	26.7 IN
Torso Depth	6.4 IN
Leg Width (Torso Width)	21.1 IN
Crotch Length (Leg Height)	36.1 IN
Leg Depth	4.2 IN

After each portion of the male figure was represented by a Crispin/Maffett cylinder, the RCS was calculated. The key aspect of this study involved the adjustment of the wavelength until the RCS total of the human reached the desired 10.76 square-feet (1 m<sup>2</sup>) from Table 2. A table of each component's corresponding contribution to the overall RCS is included. The distribution of cylinders used to model the male subject can be seen below as well.

**Table 4: RCS distribution for each component of the 95<sup>th</sup>-percentile male figure.**

<b>Component</b>	<b>RCS Value in M<sup>2</sup></b>	<b>RCS Value in FT<sup>2</sup></b>
Head	0.00382	0.0411
Torso and Arms	0.4324	4.6522
Legs	0.5638	6.0660
<b>Total</b>	<b>1</b>	<b>10.7593</b>



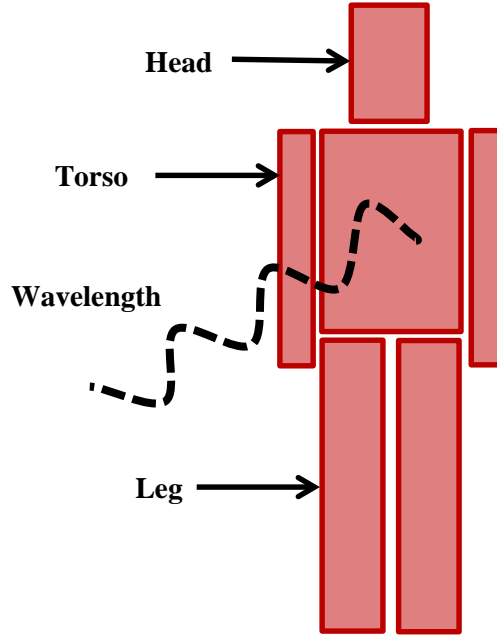


**Figure 3: Diagram of cylinders used to model a 95<sup>th</sup>-percentile male.**

The corresponding wavelength for a human male RCS of 10.76 square-feet (1 m<sup>2</sup>) was 6.8996 feet (2.1030 m). As seen in the following equation, for a constant wave velocity, the frequency is inversely proportional to the wavelength.

$$f = \frac{v}{\lambda} \quad (5)$$

With the determined wavelength of 6.9 feet, or 2.103 meters, and a wave velocity at the speed of light, 3(10<sup>8</sup>) m/s, the frequency would be roughly 142 GHz. This estimate reflects the use of High-Frequency (HF) or A-Band radar as the radar system used to track this aircraft. While the frequency is lower than most declassified types of radar known today, this lower band of frequency is being revived in the world of radar technology due to the advancements within the electronics field, especially in micronization of modern technology [11]. The estimation of wavelength, while lower than conventional systems of today, proves to be a great example of what future radar technologies may use to track and detect aerial targets.

It is important to understand that modern radar systems do operate at much higher frequencies and therefore shorter wavelengths for systems in place in hostile territory for close-range monitoring. However, at shorter wavelengths, the RCS is much smaller. Therefore, the wavelength chosen for this research can be considered as a worst case scenario. It is quite possible that systems operating in hostile territory would not use A-band radar below 900 MHz, which would be a distinct advantage to any stealth aircraft.

Overall, the 6.8996-foot wavelength from the human RCS investigation is a reasonable estimate wavelength when using Crispin and Maffett's equations. This wavelength estimate will be kept constant for the entire process of estimating RCS and provides a value of  $k$  from Equation (4). The calculation is as follows:

$$k = \frac{2\pi}{\lambda} = \frac{2\pi}{6.9} = 0.9106$$

The RCS estimation of each component is calculated as follows using Equation (3) and the now known value of  $k$ .

$$\begin{aligned}\sigma &= \frac{4}{\pi} (0.9106)^4 V^2 \left[ 1 + \frac{1}{\pi y} e^{-y} \right]^2 \\ \sigma &= (0.8755) V^2 \left[ 1 + \frac{1}{\pi y} e^{-y} \right]^2\end{aligned}\tag{6}$$

Equation (7) has been simplified to include the constant value of  $k$ . Each component of the aircraft will individually contribute a specific  $V$  and  $y$  value to fill the remaining variables of the equation.

It is important to note that Crispin and Maffett also provided equations that do not use the RCS Equation (7) from above. Other variations of these equations exist for the same shapes, and they take into account the angle at which the radar signal is impinging on the simple shape from zero

to 90-degrees. These equations can be helpful for features of the aircraft that do not lie parallel to the lateral, longitudinal, or vertical planes where the signal's angle of impingement is neither zero nor 90-degrees.

### 3. UCAV Development and Design

#### 3.1 Project Needs and Specifications Screening

The UCAV design originated from an American Institute of Aeronautics and Astronautics (AIAA) Request for Proposal (RFP) for an undergraduate student design competition. The following table describes the criteria and requirements for the UCAV as set by the AIAA RFP. As well, the full RFP document can be found in Appendix A: AIAA Request for Proposal.

**Table 5: UCAV design criteria and requirements as set by AIAA RFP.**

<b>Criteria</b>	<b>Requirement</b>
Cruise Ceiling	60000 FT
Runway Length	10000 FT
Payload (expendable)	4100 LBS
Range (unrefueled)	2000 NM at M 1.6
Cruise Mach	1.5
Dash Mach	2.0
Time to Accelerate from M 0.93 to M 2 at 50000 ft.	2 MIN (maximum)
NRE	\$10 billion
Flyaway Cost	\$200 million for 200 aircraft buy

The most important requirements set by the RFP were that the vehicle be unmanned, semi-autonomous, and combat capable with high performance. It was then added for the purposes of this research that the UCAV be designed with the minimization of the RCS in mind.

The UCAV was screened in order to better understand which requirements were the most critical to the design. The scoring chart is as follows:

	Load factors of +12/-8 vertical g's in clean config/max gross weight	Use of standard JP-8 or Jat A jet engine fuel	Augmented subsonic longitudinal static margin lies between [-5%, 10%]	Maximum C.G. excursions should not exceed 7%	Total NRE cost of less than \$10 billion (2015 dollars)	Per unit cost of less than \$200 million (2014 dollars) for 200 aircraft	Cruise ceiling: 60000 ft	Runway length: 10000 ft	Range (unrefueled): 2000 nm at M = 1.6	Cruise Mach: 1.5	Dash Mach: 2.0	Time to accelerate from M = 0.93 to M = 2.0 at 50000ft: 120 seconds	180-degree turn with weapons at M [0.85, 0.93]	Reserves for 30 min of fuel OR 10% design mission time at 10000ft/ max endurance speed	Four 1000 lb. JDAM (preferably internal)	IMPORTANCE
Unmanned	9	0	1	1	6	6	3	6	3	3	3	9	9	0	1	5
Semi-autonomous	0	0	1	1	6	6	0	1	0	0	0	3	3	1	1	5
Easy maintenance	6	6	0	0	9	9	0	0	0	1	1	0	0	1	6	1
Combat Capable	9	0	0	0	9	9	3	3	3	9	9	9	9	9	9	4
Operational Life	9	0	0	0	9	9	0	0	0	9	9	9	9	0	6	3
Cost Effective	3	0	0	0	9	9	0	0	0	3	3	0	0	0	6	4
Physical Size	6	0	1	1	9	9	3	3	6	6	6	6	6	9	9	3
High Performing	9	0	0	0	9	9	6	6	6	9	9	9	9	3	6	3
Reduced Radar Cross-Section	0	0	0	0	6	6	0	0	6	6	6	6	6	6	6	2
<b>TOTALS</b>	<b>171</b>	<b>6</b>	<b>13</b>	<b>13</b>	<b>234</b>	<b>234</b>	<b>54</b>	<b>74</b>	<b>75</b>	<b>148</b>	<b>148</b>	<b>180</b>	<b>180</b>	<b>90</b>	<b>151</b>	

**Figure 4: UCAV screening chart.**

The results from this chart show that critical factors include cost specifications, time to accelerate, the 180-degree turn with weapons, the load factors of +12/-8G, and the cruise and dash Mach values. While some of these, especially cost, were predictable, it is helpful to narrow down the most important parts of the UCAV's mission so that they can be taken into careful consideration during the preliminary design process. It is clear that a large power plant will be necessary to meet the speed requirements as well as a strong and robust structure to handle high loads. As well, the design will have to be aerodynamically efficient to ensure that range is met at the high speeds required.

### 3.2 Air Vehicle Configuration Options

From here, configuration options were weighed. It was narrowed immediately to six layout options: tailless, control-canard, flying wing, delta wing, cranked arrow and conventional configurations. An example of a tailless aircraft, sometimes coupled to include the control-canard, can be seen below.



**Figure 5: Tailless aircraft with control-canard surface.**

The control-canard was the first to be analyzed. For some designs, aircraft with control-canard can have high maneuverability due to the inherent destabilization of the aircraft by the canards. A control-canard can also counteract pitch-up moments due to tip stall by having significant nose-down deflection. This fact can be used to optimize the wing's aspect ratio and wing sweep. Close coupling to the wing also allows for directed airflow over the wings at high angles of attack to provide more lift, reduce drag, and delay stall. These attributes are especially helpful in supersonic delta wing configurations in transonic and low-speed flight regimes such as landing and takeoff. However, the use of a control-canard does come at some cost. The large, angular surface can have a negative impact on stealth characteristics due to the tendency to reflect large amounts of radar signals forward. There can also be adverse flow disturbances from the canard over the wing. After this investigation, it was clear that a control-canard could be a viable option to supplement any larger wing or fuselage design [6].

The second investigation was for tailless aircraft, also known as the flying wing, which is an excellent example of an aircraft configuration that could be used in combination with a control-canard. The B-2 stealth bomber, a modern example of a tailless aircraft, however, does not use a control canard, as seen in the figure below.



**Figure 6: The B-2 bomber aircraft, an example of a tailless configuration.**

The tailless aircraft's major downfall is the need for more control surfaces due to its inherent instability, which is why the use of a control-canard is so viable. However, the costs incurred from increasing the amount of control surfaces also increases the amount of failure points and weight on the aircraft overall. The advantages of a tailless aircraft include the removal of a horizontal stabilizer which contributes to a smaller RCS due to its sleeker profile [6].

The flying wing design also has many of the same advantages as the tailless concept including being lighter-weight and having an inherently low-parasite drag shape making it an aerodynamically and structurally efficient aircraft design. However, again, reconciling the stability problems mean including additional control surfaces, which can actually negate much of the weight and drag reductions of the original concept and make the aircraft less efficient when in yaw due to the need for spoilers or split ailerons. As well, while the slender design makes for a smaller

radar cross-section with less edges and features contributing to the RCS, it also makes it difficult for the design to meet all of the necessary specifications including payload and fuel [6].

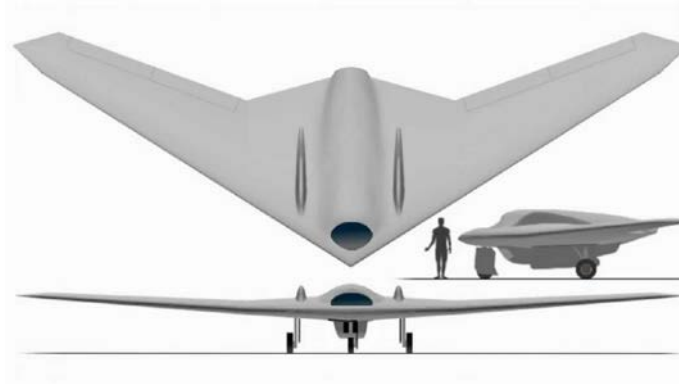


**Figure 7: Example of a tailless aircraft.**

The delta wing configuration is another option of interest for its compatibility with the control-canard. Delta wings are advantageous for their large rearward sweep. This is important for supersonic flight because it means that the shock wave boundary formed at the nose will not impinge on the wing's leading edge. This will allow the wing to continue to produce high amounts of lift. The delta wing also has a very large planform area for lift generation that contributes to low wing-loading and high maneuverability. The structure of a delta wing can also provide large internal volume for fuel or storage and can be constructed to be stronger and at much lower costs than a swept wing. However, disadvantages exist as well for the delta wing and include high induced drag and high energy bleed-off in rapid turns. A more specific type of delta wing is the cranked arrow which has two sections of the wing swept at two different angles. This reduces drag compared to the full delta wing and allows for landing at lower speeds [6].



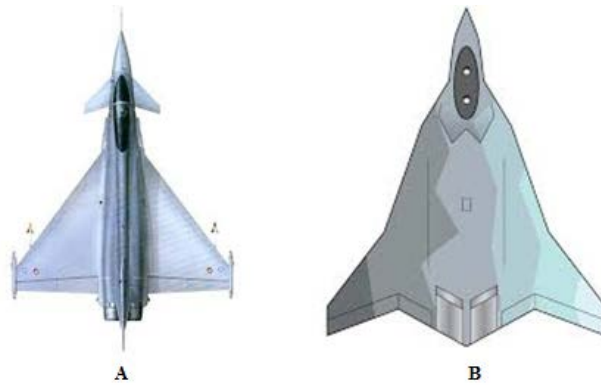


**Figure 8: Delta wing configuration (A) and cranked arrow wing configuration (B).**

Finally, the conventional configuration was considered for its versatility in many flight regimes as well as its simple design and no need for additional features that cost in weight. However, during supersonic flight, the leading edge of a conventional wing is not always behind the shockwave generated at the nose. This causes stability and control problems and air separation at high angles of attack leading to stall [6].



**Figure 9: Conventional aircraft layout of the F-22 Raptor.**

The intermediate decision was to create preliminary designs of a flying wing, cranked arrow, and conventional aircraft all having the possibility of using control-canards.

### **3.3 Final Configuration Selection**

Once the design options were narrowed down to three main configurations each with the control canard option, hand sketches were completed and scored using the Pugh method. The reference aircraft used was the Lockheed Martin F-22 Raptor. While the aircraft met the performance requirements for the comparison, it is not unmanned, and therefore is impossible to compare for the semi-autonomous requirement. While the aircraft is very combat capable and has a long operational life, the F-22 also does not have a comparable goal for being a cost effective weapons acquisition program. According to the 2011 Defense Acquisitions Assessment from the Government Accountability Office, the F-22 Raptor had a final procurement cost of \$412 million each for 183 aircraft. This nearly doubles the goals for this UCAV project and supersedes initial estimates for the Raptor program itself [7]. Overall, the Raptor is a larger fighter aircraft with high performance capabilities and excellent stealth qualities. Because no unmanned combat vehicle exists today, the Raptor is the best reference vehicle with which to complete the scoring process.

The remaining design configuration options were scored, and the figure at the end of this section demonstrates how well each design competed against the F-22 reference as well as each other. All design configurations would meet the unmanned and semi-autonomous categories in full unlike the F-22 reference. For combat capabilities, the conventional aircraft scored much lower than the flying wing and cranked arrow due to its lack of internal loads capacity. The shapes of the cranked arrow and flying wing have a large internal volume such that fuel and ordnance can both be entirely internal. This allows for better handling in flight, reduced overall drag, and smaller RCS.

As for operational life, all aircraft scored equally since each configuration would be designed to be easily maintainable and structurally sound. However, the configurations varied in scoring for cost effectiveness. Because the flying wing has not been tested as extensively in supersonic flight, it would take more research and development to build the knowledge base and technology for the flying wing to be effective at those high speeds. On the contrary, the conventional and cranked arrow configurations have both been heavily studied for supersonic flight and would require less research and development investment.

The physical size of the aircraft configurations was also considered. Because supersonic flight requires more purpose-shaping using the ideal Sears-Haack body as a reference, the flying wing suffered in this category. This is due to the fact that a flying wing would need to be very large in order to be effective at supersonic speeds. The conventional and cranked arrow configurations, however, would be more compact while still being effective at supersonic speeds.

The performance aspect was also rated for each configuration. Again, the flying wing was rated quite a bit lower relative to the other two configurations because of its lack of control authority. While all of the designs may be inherently unstable for combat-performance purposes, the flying wing has less control surfaces to exert control over the aircraft while maneuvering. This means that the flying wing is not as agile an option as the cranked arrow and conventional crafts.

Finally, the radar cross-section was rated for each of the aircraft configurations. Because radar cross-section reducing technologies exist in many forms from radar-absorbing paint to low-probability-of-intercept radar on-board the vehicle, each aircraft was rated close to each other in

value. The shaping of the aircraft greatly impacts the vehicles observability on enemy radars, and therefore distinctions between the three were made. The conventional configuration simply does not fare well in this category due to its protruding wing and stabilizer surfaces. However, since the flying wing design has a smooth and blended fuselage shape, it has the lowest radar cross-section of the three designs. The cranked arrow is somewhere between the two others.

The scoring chart can be seen below with each design, the F-22 reference, and all of the relevant categories used to score each aircraft. Overall, the cranked arrow was the most viable candidate for the UCAV design and was chosen as the basis for the rest of the design process.

		Reference A		Design B		Design C		Design D	
		F-22 Raptor		Flying Wing		Cranked Arrow		Conventional	
Needs	Weight	Rating	Weighted Score	Rating	Weighted Score	Rating	Weighted Score	Rating	Weighted Score
Unmanned	17.2%	0	0.00	5	0.86	5	0.86	5	0.86
Semi-autonomous	17.2%	0	0.00	5	0.86	5	0.86	5	0.86
Combat Capable	13.8%	5	0.69	3	0.41	5	0.69	1	0.14
Operational Life	10.3%	5	0.52	5	0.52	5	0.52	5	0.52
Cost Effective	13.8%	3	0.41	2	0.28	3	0.41	3	0.41
Physical Size	10.3%	5	0.41	1	0.10	5	0.52	5	0.52
High Performing	10.3%	5	0.52	2	0.21	5	0.52	5	0.52
Reduced Radar Cross-Section	6.9%	4	0.39	5	0.34	5	0.34	4	0.28
Total Score		2.90		3.59		4.72		4.10	
Rank		4		3		1		2	
Continue?		No		No		Yes		No	

**Figure 10: UCAV scoring chart.**

### 3.4 QF-36 Concept

The final configuration was used as an initial idea of the overall shape of the now-designated QF-36, nicknamed “Thunder”. The QF-36 was named for its drone and fighter role denoted by the QF. The number 36 and nickname “Thunder” pay homage to the F-35 Lightning II Joint Strike Fighter (JSF) since a UCAV-type acquisition program would most likely follow after JSF comes to a close, much like thunder is heard after lightning.

The final layout of the QF-36 can be seen below. The main inspiration for this aircraft was the SR-71 reconnaissance aircraft, but executed on a smaller scale and without a cockpit. This allowed for a streamline body with large, smooth wing surfaces, and room for two powerful engines and ample fuel and internal stores.

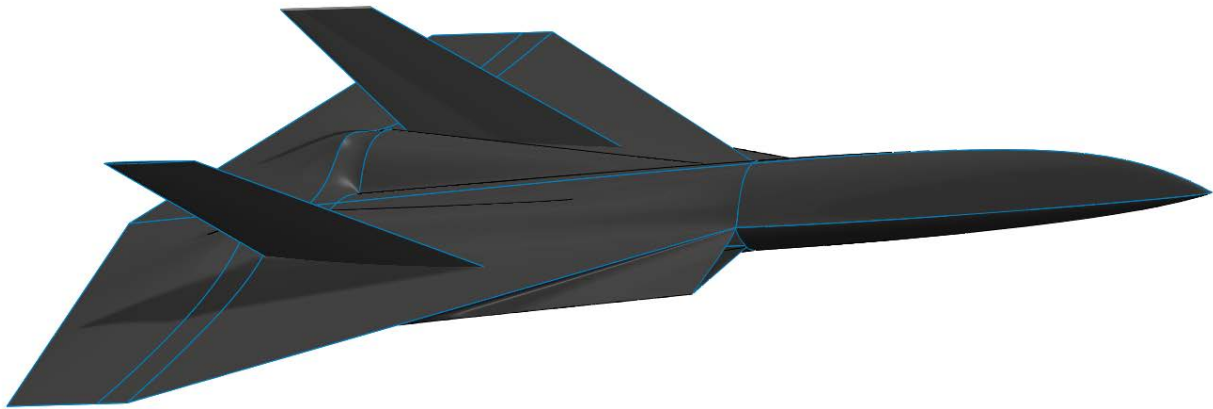


**Figure 11: QF-36 Thunder concept.**

## 4. Radar-Cross Section Calculations

### 4.1 UCAV Profile Selection

In order to remain within the timeframe of completion for this research, the UCAV was to be analyzed from two angles, or views. The first was the head-on view, or front-view. This was selected for the front view's relevance when approaching hostile territory. As the UCAV approaches the enemy, the radar systems would detect the UCAV from the front looking aft (FLA). This scenario is one of the most typical that a combat aircraft would face when deployed. The second view chosen for analysis was the side-view. If the UCAV would have a mission to fly parallel along enemy territory, the side-view would be detected from the perspective of the enemy radar. It is therefore important that for both of these views, the RCS be minimized so as to evade detection from the enemy for as long as possible. The bottom view of the aircraft was not chosen for analysis due to the short time period that the underside of the vehicle would be visible by enemy radar directed upward. By the time the vehicle would be detected and its presence understood, the UCAV would have completed its mission and evacuated the territory.

### 4.2 Front-View RCS Estimation

The first calculation used the front-view of the UCAV as seen below:

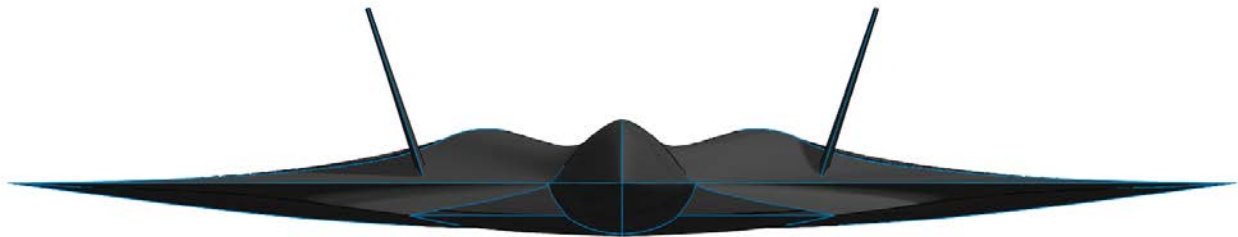


**Figure 12: Front-view of UCAV.**

This iteration of RCS calculation began by analyzing the most straightforward shape of the craft: the fuselage. The fuselage is considered to be the body of the aircraft from the nose to the front of

engine inlets which is more easily seen in Figure 11. The shape chosen for this fuselage was the lens, or ogive.

Once the ogive shape was selected, it was necessary to match the correct size to the profile and shape of the UCAV fuselage. First, an equation for the ogive was found to plot its profile in the X-Y plane as a means of comparison to the fuselage shape. The equation for an ogive is given as:

$$y = \sqrt{\rho^2 - (L - x)^2} + R - \rho \quad (7)$$

For this shape,  $\rho$  is the radius of the larger circle that makes up the profile edge of the lens. It is expressed as:

$$\rho = \frac{R^2 + L^2}{2R} \quad (8)$$

The length of the fuselage is 25 feet up to the engine inlets, and therefore  $L$  was set as a constant of 25. The remaining variable was  $R$  was varied to compare to the size and shape of the actual UCAV fuselage design. The closest values of  $R$  that nearly met the shape of the UCAV were between two and 2.75 feet. The plot in Figure 13 is of the actual profile of the fuselage and ogive shapes. The profile from zero to ten feet is not exactly met by the ogive estimation, however, as the fuselage lengthens, the ogive shape better matches the profile. Based on radii variations alone, it is unclear from Figure 13 as to which ogive shape best meets the fuselage shape.

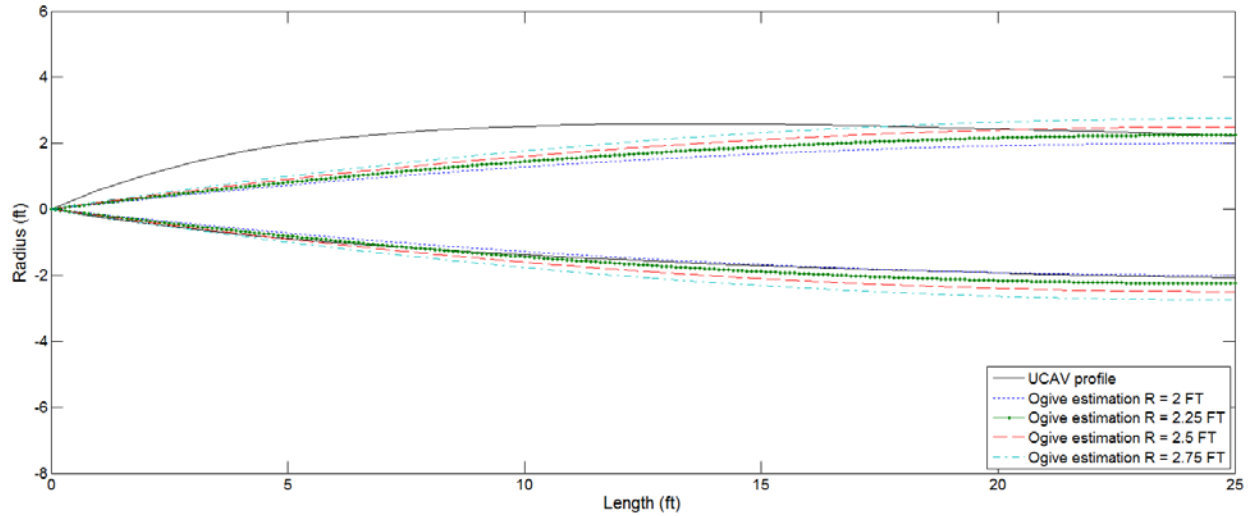


**Figure 13: Ogive and fuselage profile comparison with varying radii.**

It was clear more investigation was necessary to optimally pick an ogive. When estimating the RCS of an object using simple shapes, volume is one of the most important factors to match. In order to best take into account the volume of the fuselage, cross sections were calculated from the UCAV SolidWorks model at one foot intervals. The collection of these cross-sectional areas in a Riemann sum accounted for a volume estimate that shows the variation of volume with x-distance from the nose of the aircraft. This would allow for the most appropriate shape estimate or size of a given shape to be chosen to calculate the RCS. This fuselage volume analysis was then compared with the same four ogive shapes with radii from two to 2.75 feet as previously shown in Figure 13. From the new plot seen in Figure 14, it was much clearer as to which ogive best matched the fuselage in volume.



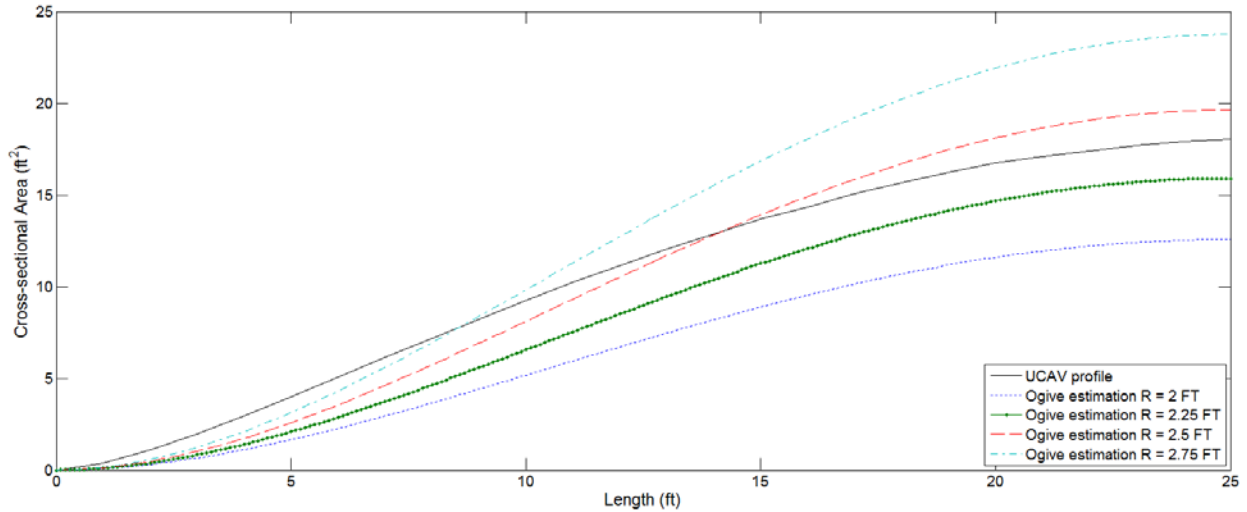


**Figure 14: Ogive and fuselage cross-section comparison with varying radii.**

The fuselage was best represented by the ogive with a radius of 2.5 feet. While the ogive cross-sectional area is slightly below the fuselage from zero to 14 feet, it makes up for the losses from 14 to 25 feet. The estimation was then sufficient enough to predict the RCS contribution from the fuselage.

The aforementioned work is proof that the ogive is an excellent shape to be used when estimating the forward fuselage. However, new equations, variables, and coordinate systems are used to calculate the ogive RCS. All of these equations share similar names and variables, however, the following calculations refer to the labels in the Figure 15.

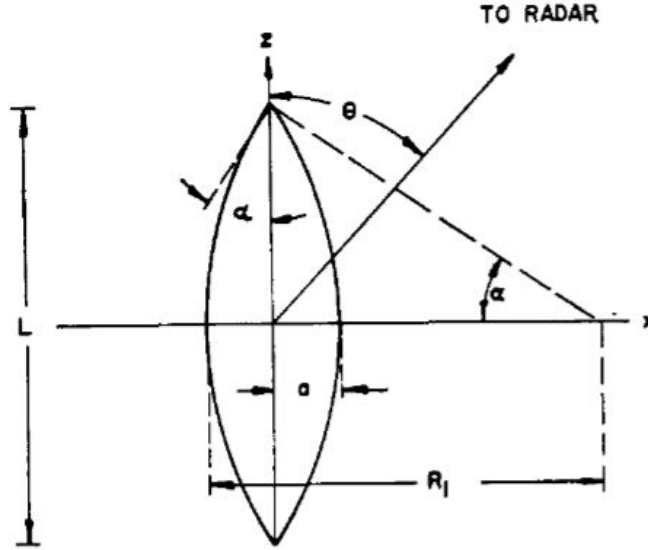


**Figure 15: Ogive coordinate system and labels for side-view RCS estimation.**

Unlike the ogive-lens estimation from Table 1, this new coordinate system seen in Figure 15 relies on a different equation to estimate the shape's RCS. Equation (10) is true for varying values of theta from zero to  $(90 - \alpha)$  degrees.

$$\sigma = \frac{(R_1 a) \lambda^2 \tan^4 \alpha}{16\pi \cos^6 \theta (1 - \tan^2 \alpha \tan^2 \theta)^3} \quad (9)$$

Because theta is equal to zero for the fuselage in the front-view, Equation (10) can be reduced to following:

$$\sigma = \frac{(R_1 a) \lambda^2 \tan^4 \alpha}{16\pi} \quad (10)$$

An important change has been made to the previous two equations that was not reflected in the study by Crispin and Maffett. These equations provided in the Crispin/Maffett study did not have the correct units of RCS in the report and, after much deliberation, were adjusted to include the sizing parameters of the width and radius. The product of these two parameters were multiplied to the numerator of Equation (10) in order to reflect the correct units of RCS. This decision was made based on other equations provided within the same report.

With this new expression, an RCS value for the fuselage was calculated using the following defined variables including the wavelength estimated earlier to be 6.9 feet. As well, using the top view of the aircraft, alpha ( $\alpha$ ) can be measured to be 13.69°. Using Equation (13) and the known values of the wavelength and alpha ( $\alpha$ ), the RCS contribution from the forward fuselage can be calculated and seen in Table 6 below.

**Table 6: Front-view estimated values for forward fuselage.**

Variable	Value
$\lambda$	6.8996 [FT]
$R_1$	105.67 [FT]
$a$	3.00 [FT]
$\alpha$	13.69°
$\sigma$	<b>1.0570 [FT<sup>2</sup>]</b> <b>0.982 [M<sup>2</sup>]</b>

The next calculations were those of the tails. The flat plate is an adequate shape for modeling leading edges of wing and fin surfaces and represents the surface as a collection or summation of thin wires [4]. The equation for a square flat plate is as follows:

$$\sigma = \frac{4\pi a^4}{\lambda^2} \left[ \frac{\sin(ka \sin \theta)}{ka \sin \theta} \right]^2 \quad (11)$$

For the flat plate, the coordinate plane is set such that when the radar is impinging the plate perpendicular to its surface, theta is equal to zero. Therefore, at the edge of the plate, radar is impinging the surface at a theta equal to 90-degrees. Since the tails are mounted parallel to the fuselage nose such that in the front view, theta is equal to 90-degrees, the flat plate equation can be further simplified.

$$\sigma = \frac{4\pi a^4}{\lambda^2} \left[ \frac{\sin(ka \sin \theta)}{ka \sin \theta} \right]^2 = \frac{4\pi a^4}{\lambda^2} \left[ \frac{\sin(ka)}{ka} \right]^2 \quad (12)$$

This equation refers to both wavelength ( $\lambda$ ) and  $k$  as solved for previously. As well, Equation (14) includes the value  $a$ , which refers to the characteristic side length of the square plate. Again, the role of similar volume and area is taken into account when using the dimensions of the tail. The tail area is 57.97 square feet, and therefore a square of side length 7.6138 has the equivalent area. This will be used as the representative side length for the tail RCS estimation.

**Table 7: Front-view estimated values for tail surfaces.**

<b>Variable</b>	<b>Value</b>
$\lambda$	6.8996 [FT]
$k$	0.6767 [FT <sup>-1</sup> ]
$a_{tail}$	7.7440 [FT]
$\sigma$	<b>0.2877 [FT<sup>2</sup>]</b>

Therefore, using the previous information and characteristic lengths calculated, each tail's RCS contribution is equal to 0.1592 square feet.

Aft of the fuselage nose is the blended wing-body. In order to estimate these components together in the front view, the lens shape was used for its similarity to the wing profile from the FLA. This entailed the use of the ogive again as was done for the fuselage nose.

From the previous estimation, Equation (10) was used because it was accurate near low values of theta. However, as seen in Figure 15, theta was no longer equal to zero. Using the assigned coordinate system, the value of theta was 90-degrees since the radar was impinging from the side. This entailed using a new equation for the ogive RCS estimation. According to Crispin and Maffett, the equation valid near theta values of 90-degrees is as follows:

$$\sigma = \pi R_1^2 \left[ 1 - \frac{R_1 - a}{R_1 \sin \theta} \right] \quad (13)$$

Since theta was equal to 90-degrees, and the equation reduced as follows:

$$\sigma(\theta) = \pi R_1^2 \left[ 1 - \frac{R_1 - \alpha}{R_1 \sin \theta} \right] = \pi R_1^2 \left[ 1 - \frac{R_1 - \alpha}{R_1} \right] = \pi \alpha R_1$$

The CAD drawing provided the measurements needed to calculate the estimated RCS. The ogive shape was estimated to best fit the curvature of the underside of the UCAV. This resulted in an alpha ( $\alpha$ ) value equal to 8.5°. This did not match the top of the UCAV shape as well, but it was an acceptable compromise considering future plans for estimating the engine nacelles. The table of values and final RCS estimation for the wing-body using the ogive to calculate RCS can be seen below:

**Table 8: Front-view estimated values for wing surfaces.**

Variable	Value
$\theta$	90°
$\alpha$	8.91°
$R_1$	3222.99 [FT]
$a$	3.89 [FT]
$\sigma$	<b>1975.5864 [FT<sup>2</sup>]</b> <b>183.605 [M<sup>2</sup>]</b>

From these estimations, it is clear that the use of the ogive to estimate the wing-body as a whole is not appropriate. Other alternatives in estimations include the lens and the cone spheroid, however, upon further investigation, these simple shapes were also a poor estimation of the wing-body portion of the UCAV and grossly overestimated the wing-body RCS even more so than the ogive. It was therefore necessary to divide the wing-body into more simple shapes for estimation.

The next decision involved reusing the flat plate estimation for the wing-body as done for each tail. The useful wing area relevant to the front-view was determined from the CAD drawing, and Equation (14) was used to find the RCS contribution.

**Table 9: Front-view estimated values for the wing.**

<b>Variable</b>	<b>Value</b>
$\lambda$	6.8996 [FT]
$k$	0.6767 [FT <sup>-1</sup> ]
$A_{wing}$	681.92 [FT <sup>2</sup> ]
$a_{wing}$	26.1136 [FT]
$\sigma$	<b>35.2939 [FT<sup>2</sup>]</b> <b>3.280 [M<sup>2</sup>]</b>

The wing contribution was 35.2939 square-feet (3.280 m<sup>2</sup>). While still much larger than the rest of the previously estimated surfaces, it is obvious that by breaking up the wing-body section, the RCS estimation is much more reasonable.

The last main contributor to the front view RCS was the engine nacelles, which are imbedded into the wing-body but protrude above the main wing surface. The spindle shape best represented these protrusions. Using the CAD drawing, the dimension of these engine nacelles were determined and the RCS was calculated.

**Table 10: Front-view estimated values for the engine nacelles.**

Variable	Value
$k$	0.9107 [FT <sup>-1</sup> ]
$c$	3.1117 [FT]
$d$	2.1990 [FT]
$V$	1.1320 [FT <sup>3</sup> ]
$y$	50.4228
$\sigma$	<b>1.1222 [FT<sup>2</sup>]</b> <b>0.1043 [FT<sup>2</sup>]</b>

The engine nacelle RCS contribution is therefore 1.1222 square-feet (0.1043 m<sup>2</sup>) each. Having completed the estimation from this angle of detection, the RCS for each component was summed providing the total front-view RCS for the QF-36.

**Table 11: Total RCS of the QF-36 in the front-view.**

Aircraft Component	RCS Value
Forward Fuselage	1.0570 [FT <sup>2</sup> ]
Wing	35.2939 [FT <sup>2</sup> ]
Tail (each)	0.2877 [FT <sup>2</sup> ]
Engine Nacelle (each)	1.1222 [FT <sup>2</sup> ]
<b>Total</b>	<b>39.1707 [FT<sup>2</sup>]</b> <b>3.640 [M<sup>2</sup>]</b>

This estimate is well within the large fighter range as seen in Table 2.

### 4.3 Side-View RCS Estimation

The next set of calculations for the first-iteration UCAV design calculated the RCS of the side-view as seen below:



**Figure 16: Side-view of UCAV**

By returning to the flat plate theory for the tails, the same Equation (13) was used with a new value of theta. The tails are offset at an angle of 18.43-degrees outward which changes the value of theta in Equation (13); the simplified Equation (14) is no longer valid for this scenario. Therefore, the RCS of the single tail surface in the side view is estimated using the following information, most of which remains the same from the front-view estimation:

**Table 12: Side-view estimated values for the tail.**

Variable	Value
$\theta$	18.43°
$\lambda$	6.8996 [FT]
$k$	0.9107 [FT <sup>-1</sup> ]
$a_{tail}$	7.7440 [FT]
$\sigma$	<b>0.2890 [FT<sup>2</sup>]</b> <b>0.0269 [M<sup>2</sup>]</b>

Again, the wing was also be taken into account by using the same flat plate estimation as aforementioned. In the side-view, the useful wing area was smaller than the front-view estimation, and the RCS changed to reflect that.

**Table 13: Side-view estimated values for the wing.**

Variable	Value
$\lambda$	6.8996 [FT]
$k$	0.6767 [FT <sup>-1</sup> ]



$A_{wing}$	574.40 [FT <sup>2</sup> ]
$a_{wing}$	23.97 [FT]
$\sigma$	<b>25.2718 [FT<sup>2</sup>]</b> <b>2.349 [M<sup>2</sup>]</b>

The fuselage in the side-view proved to be much more difficult to predict. In addition to the ogive method used in the front-view for the fuselage nose, Crispin and Maffett also developed equations to predict the same ogive with radar signals impinging the shape perpendicularly. However, the use of these equations resulted in an RCS near 1000 square-feet (about 92 m<sup>2</sup>) for the wing-body. Upon further investigation, it was determined that this ogive shape was useful for the fuselage nose estimation because the rear of the shape was in shadow. However, because to the curvature of the fuselage in the side-view was less uniform than the standard ogive, the choice was made to divide up the fuselage into multiple spindles. This would better take into account more nuances of the design.

The spindle was chosen as the next best alternate to predict the fuselage RCS from the side-view because of its similarity to the ogive. The flat surface on the spindle allows more flexibility in modeling the top and bottom of the fuselage separately. Using this method, two spindles represented the fuselage nose and engine nacelle and a third represented the underside of the fuselage from nose to aft. The RCS of each spindle is as follows:

**Table 14: Fuselage represented by multiple spindles in the side view.**

<b>Aircraft Component</b>	<b>RCS Value</b>
Fuselage (Top/Forward)	15.6655 [FT <sup>2</sup> ]
Fuselage (Top/Aft)	26.8001 [FT <sup>2</sup> ]
Fuselage (Undercarriage)	97.4523 [FT <sup>2</sup> ]
<b>Total Fuselage</b>	<b>139.918 [FT<sup>2</sup>]</b> <b>13.00 [M<sup>2</sup>]</b>

It is clear from this analysis that the use of the spindle as an estimation of multiple portions of the fuselage is much better than the ogive estimation of the entire aircraft fuselage. Unfortunately, the spindle shape exposes just how high the fuselage contribution is in the side-view. The overall RCS for the QF-36 in the side-view is as follows:

**Table 15: Total RCS for the QF-36 in the side-view.**

<b>Component</b>	<b>RCS Value</b>
Total Fuselage	139.918 [FT <sup>2</sup> ]
Wing	25.2718 [FT <sup>2</sup> ]
Tail	0.2890 [FT <sup>2</sup> ]
<b>Total</b>	<b>165.4787 [FT<sup>2</sup>]</b> <b>15.379[M<sup>2</sup>]</b>

The penalty taken by the high RCS fuselage is seen immediately in the side-view estimation; the side-view estimation RCS is nearly triple of the front-view.

## 5. Discussion and Design Implications

The development of this tool used to predict an aircraft's RCS was proven successful by the trial previously described. Not only were the results reasonable estimations, but they revealed patterns that have been predicted in open source literature. According to some sources, there do exist declassified RCS values for current and past aircraft. A list of these aircraft and their respective RCS values is as follows and includes the comparison to the QF-36.

**Table 16: Various RCS estimations for past and present military aircraft as well as the QF-36 concept.**

<b>Aircraft</b>	<b>View</b>	<b>RCS Value in M<sup>2</sup></b>	<b>RCS Value in FT<sup>2</sup></b>
F-22A Raptor	Generalized	0.00018	0.0019
F-35A Lightning II	Generalized	0.00143	0.015
F-117A Nighthawk	Generalized	0.001 to 0.01	0.01 to 0.1
B-1B Lancer	Frontal	1	11
F-4 Phantom II	Frontal	6	65
B-1A Excalibur	Frontal	10	110
T-33 Shooting Star	Frontal	10	110
T-33 Shooting Star	Side	100	1100
B-70A Valkyrie	Frontal	40	430
B-70A Valkyrie	Side	10 <sup>5</sup> +	10 <sup>6</sup> +
B-52 Stratofortress	Frontal	100	1100
<b><i>UCAV QF-36 Thunder</i></b>	<b><i>Frontal</i></b>	<b><i>3.7</i></b>	<b><i>40</i></b>
<b><i>UCAV QF-36 Thunder</i></b>	<b><i>Side</i></b>	<b><i>15.3</i></b>	<b><i>165</i></b>

While this table serves as a decent resource of RCS values for several vehicles, it is important to understand that because the wavelength used to calculate these RCS values is unknown, this is not an ideal means of comparison. This table serves as a basis for understanding where specific aircraft lie, but there is the chance that each RCS was calculated using different radar systems based on the technology relevant during their era of operation. For instance, the B-52 RCS could have been calculated by radar systems relevant to the period in which the Stratofortress entered

service which was in 1955. On the other hand, the F-22 signature could be estimated using radar relevant to today's technological standards. While there is little that can be done to solve this problem, the information still proves that the QF-36's RCS predictions are on the correct scale.

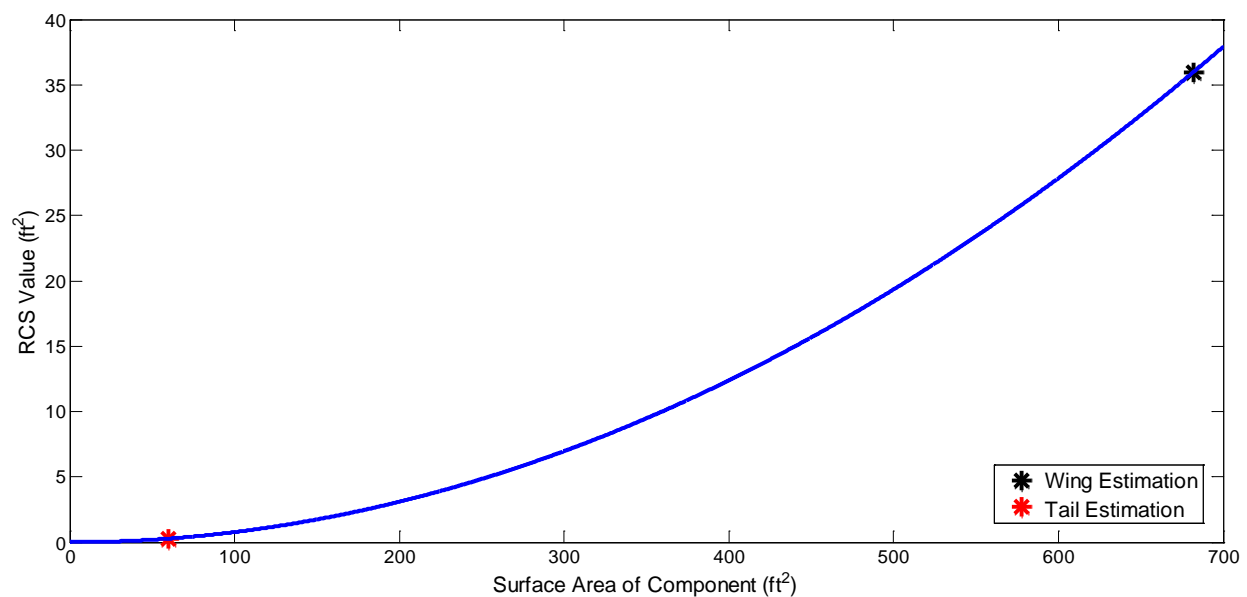
The F-22 RCS was calculated based on a USAF news release claiming that the Raptor's RCS was that of a 15 millimeter diameter marble. Years later, the F-35 RCS was said to be that of "about a golf ball" with a diameter of 4.3 centimeters [16]. What is important to keep in mind is that vehicles including the F-22 and F-35 among others have other means of reducing their RCS values through radar absorbing paint and onboard low-probability-of-intercept radar systems in addition to purpose-shaping of the fuselage. It is unknown by how much radar absorbing paint and other systems will further lower an aircraft's RCS.

Table 15 shows how the QF-36 fits within the other jets and their known RCS estimations. The wingspan of the QF-36 is 50 feet compared to the F-4's 38 feet and F-117A's 43 feet, and the QF-36's has an RCS that lies between that of the stealth jet and the fighter with respect to the front-view. It is clear that the side-view of the QF-36 is rather high as it is near the T-33 side view RCS value. However, the T-33 is only 38 feet compared to the QF-36's 70 foot length.

With respect to the results, while the larger surfaces usually lend themselves to higher RCS values, the tails proved to be the most unexpected feature. As seen in Table 11 and Table 14, the tails had very small contributions to the overall RCS of the aircraft. Even on the broad side of the QF-36, the protruding tails contributed little to the total RCS. Both the wing and the tail RCS values were predicted using the flat plate equations, however, their impact on a specific view's RCS was varied.

The wing made up 90-percent of the front-view RCS and 15-percent of the side-view. On the contrary, the tail only made up 0.7-percent and 0.2-percent of the front- and side-view RCS values, respectively. As well, even in the side-view, where a much larger surface area of the tail was exposed, the tail RCS only changed by 0.5% from the front-view.

The following plot reveals the how the flat plate RCS estimation varies with increasing surface area of the modeled component at a zero-degree incidence angle. In other words, the radar is impinging the surface at its edge rather than its broad side.



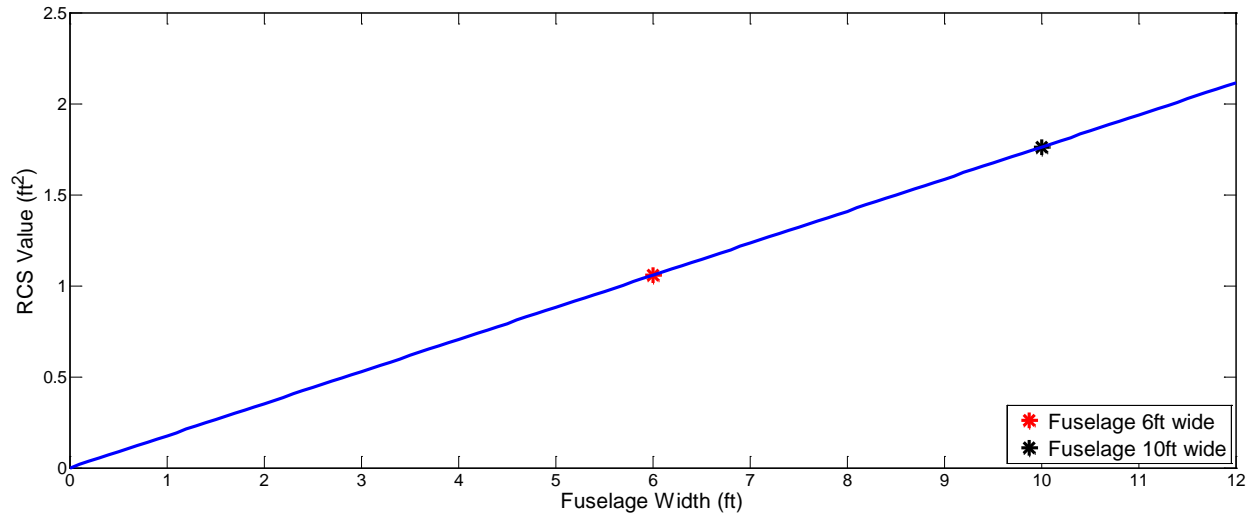
**Figure 17: Flat plate RCS estimation with tail and wing front-view examples.**

As seen in the plot in Figure 17, the relationship between surface area and RCS is exponential. Since the tail and wing differ drastically in size, this relationship between surface size and RCS is important. The wing and tail surfaces are the two most crucial aspects of an aircraft. This is especially true for the QF-36 since the UCAV has no need for a cockpit or any human factors-related design features. These observations prove that changes to the tail and wing will impact the overall RCS much differently. The results prove that even with large tail surfaces, the RCS

contribution is always going to be much lower than the wing. It is therefore in a design engineer's best interest to minimize wing size and maximize tail size when meeting performance specifications. With tails, larger horizontal stabilizers and rudders (or for this aircraft, a "ruddervator") provide for a more maneuverable the craft. Because the impact of the tail RCS is so low, even drastic changes to the tail sizing will have a low impact on the RCS. Designers do not have to compromise on performance objectives like spin recovery and tight turn radii. As well, since the elevator can be rather large and no human is in the cockpit, the UCAV can meet its high G load requirements at little cost to the RCS.

On the contrary, the exponential increase in RCS with surface area means that a large wing causes a massive RCS contribution for each view. From a design perspective, this encourages the minimization of the wing size which leads to smaller control surfaces and lessened roll performance. Smaller wings also lessen the amount of fuel able to be carried internally onboard the aircraft. With a high cruise and dash Mach number as well as a considerable range goal as set by the AIAA RFP, the loss of volume for fuel could be crucial to meeting mission objectives.

In order to make up some of the losses in wing volume, a compromise can be made while increasing the size of the fuselage. In the front-view, the fuselage only makes up 2.7-percent of the total RCS for that view. For the side-view, the fuselage constitutes 85-percent. This drastic difference suggests how the point of the fuselage shape diffuses the radar signal well, whereas the side-view reflects much of the signal back to the receiver. The length of the aircraft can be changed and with goals for a smaller wing, this is a plausible design option to consider. However, in order to regain the fuel volume lost in the wings, it is possible to widen the fuselage at a low RCS penalty.



The previous plot shows that the change in fuselage width has a linear relationship to the RCS, but even for an unreasonably large, ten-foot wide fuselage, the RCS increased by 67-percent to a mere 1.767 square-feet (0.1642 m<sup>2</sup>). This is still a meager five percent of the total front-view RCS. This allows for the volume of the fuselage to be adjusted to accommodate any payload of fuel and radar systems with little increase to the RCS. Unfortunately, the spindle used to estimate the side-view of the fuselage does not taken into account the depth of the fuselage at that angle, only the height and width. This would be an excellent start to a further investigation of the fuselage shape and its impact on the RCS. Without a cockpit in the design, new fuselage shapes could be explored in ways never before attempted.

Another possibility regarding the wing deals with the way in which it was modeled. The initial attempt at calculating the RCS of the wing involved using total wing area seen forward looking aft. This involved calculating the port and starboard wings as one, square flat plate. However, looking aft, by modeling the wing as one instead of two surfaces, the estimation included a portion of the wing that lies in shadow of the fuselage nose. As a further investigation, the wing was then modeled as two separate flat plate surfaces in an attempt to compare it to the single plate model.

The resulting RCS of each wing was 9.0828 square-feet ( $0.8441 \text{ m}^2$ ) making the total wing RCS 18.1656 square-feet ( $1.6883 \text{ m}^2$ ). This is a reduction in wing RCS of nearly 50-percent. This shows how by modeling each component with more and more detail, a more thorough and accurate RCS of the total aircraft can be calculated. While less shapes and less detail capture the initial RCS, the more effort that goes into modeling each component will surely produce a more accurate RCS. This may result in the fluctuation of each view's RCS.



## 6. Conclusion

This research demonstrates the feasibility of predicting an aircraft's radar echo, or RCS, using open-source equations for simple shapes. Because of the classified and time-consuming nature of calculating exact RCS values, this tool could be used throughout the aircraft design process as a means of understanding which components of the vehicle contribute the most to the overall RCS. Not only does this tool save time and effort, but it also provides the designer with more information earlier in the design process. Stealth is one of the newest frontiers relevant to aircraft design and will continue to be so long as radar remains relevant. With this in mind, any tools created to help integrate new design techniques relevant to stealth are important as they streamline the efforts of designers and alleviate their workload. It is for these reasons among others that this research has relevance to the current field of military aircraft design.

With respect to the QF-36, the methodology developed for calculating RCS gave insight into which areas of the aircraft to concentrate efforts in order to reduce the overall RCS. While its RCS was a reasonable value compared to other craft, the UCAV's unique and pilotless mission allow for adjustments to further reduce the RCS. To accommodate more fuel and stores, a high fuselage volume can be made with little increase in the overall signature size. As well, it is clear that a compromise will need to be made with regards to the control surface sizing. The wing has a high contribution of RCS in both the front- and side-views. In contrast, however, the tails contributed much less than expected in both analyses of RCS. This allows for maximized turn and spin recovery performance with next to no impact on the RCS. These observations are crucial to realizing the power of this tool. In future iterations of the QF-36, more and more detailed analyses

of components can be completed leading to a more refined and intelligently designed aircraft concept.

## References

- [1] Skolnik, Merrill I., "Radar (electronics)," *Encyclopedia Britannica Online*, 2 Aug 2013. Web. 09 Sept 2014, <http://www.britannica.com/EBchecked/topic/488278/radar>.
- [2] "Stealth Technology and the Counter-stealth Response." *Air Force Technology*. Kable Intelligence Limited, 25 Aug. 2011. Web. 08 Sept. 2014, <http://www.airforce-technology.com/features/feature128011/>.
- [3] Cadirci, Serdar, "RF Stealth (or Low Observable) and Counter-RF Stealth Technologies: Implications of Counter-RF Stealth Solutions for Turkish Air Force," Naval Postgraduate School, 2009.
- [4] Crispin, J. W., Maffett, A. L., "Radar Cross-Section Estimation for Simple Shapes," *Proceedings of the IEEE*, 1965.
- [5] Dimitris V. Dranidis, "Airborne Stealth in a Nutshell-Part I," the Magazine of the Computer Harpoon Community <http://www.harpoonhq.com/waypoint/>. (Accessed February 2015).
- [6] Roskam, Jan. *Airplane Design*. Vol. Part 1: Preliminary Sizing of Airplanes. Ottawa: Roskam Aviation and Engineering Corporation, 1985. Print.
- [7] United States. Government Accountability Office. Defense Acquisitions Assessment of Selected Weapons Programs. By Michael J. Sullivan. 2011. Print. GAO-11-233SP.
- [8] "The Electromagnetic Spectrum: Radio Waves." *NASA Science Headquarters*. Web. 12 Dec 2015, <http://science.hq.nasa.gov/kids/imagers/ems/radio.html>.
- [9] "Low-frequency radar," *Wikipedia*, 26 Jan 2016. Web. 28 Jan 2016, [https://en.wikipedia.org/wiki/Low-frequency\\_radar](https://en.wikipedia.org/wiki/Low-frequency_radar).

- [10] O'Donnell, Robert M., "Radar Systems Engineering, Lecture 7 – Part 1, Radar Cross Section", *IEEE New Hampshire Section*, 2010.
- [11] Wolff, Christian, "Waves and Frequency Ranges", *Radar Basics*. Web. 1 Feb 2016, <http://www.radartutorial.eu/07.waves/Waves%20and%20Frequency%20Ranges.en.html>.
- [12] Wolff, Christian, "MEADS", *Card Index of Radar Sets - Battlefield*. Web. 1 Feb 2016, <http://www.radartutorial.eu/19.kartei/karte410.en.html>.
- [13] Anthropometry and biomechanics, Web. 15 Feb 2016. [http://www.ergo-eg.com/uploads/digi\\_lib/116.pdf](http://www.ergo-eg.com/uploads/digi_lib/116.pdf)
- [14] "Anthropometry and Biomechanics Related Design Data", *NASA Man-Systems Integration Standards*. Web. 15 Feb 2016. <http://msis.jsc.nasa.gov/sections/section03.htm>
- [15] Hott, Bartholomew, Pollock, George E. "The Adevent, Evolution, and New Horizons of United States Stealth Aircraft." Web. 18 Feb 2016. <http://web.ics.purdue.edu/~gpollock/The%20Advent,%20Evolution,%20and%20New%20Horizons%20of%20United%20States%20Stealth%20Aircraft.htm>
- [16] "RCS of Typical Radar Targets". Web. 31 March 2016. [http://www.alternatewars.com/BBOW/Radar/Radar\\_Targets.htm](http://www.alternatewars.com/BBOW/Radar/Radar_Targets.htm)

## **Appendix A: AIAA Request for Proposal**

# 2014-2015 AIAA Foundation Undergraduate Individual Aircraft Design Competition

## Uninhabited Long Range Strike Vehicle

### I. Rules – General

1. All AIAA Student Members are eligible and encouraged to participate.
2. Students may **NOT** participate on more than one team in any one design competition category. However, a student may participate in multiple design categories.

For example, a student **MAY** participate in both the Undergraduate Team Aircraft competition and the Undergraduate Team Space Transportation competition; but that student may **NOT** participate on two teams in the Undergraduate Team Space Transportation competition.

3. Students must submit their final report via email to AIAA Student Programs (Rachel Andino, [rachela@aiaa.org](mailto:rachela@aiaa.org)). It is the team's responsibility to ensure delivery of the final report to AIAA. We recommend utilizing the return receipt option for validation.
4. *A "Signature" page must be included in the report and indicate all participants, including faculty and project advisors, along with students' AIAA member numbers and signatures.* Designs that are submitted must be the work of the students, but guidance may come from the Faculty/Project Advisor and should be accurately acknowledged.

5. Each proposal should be no more than 100 double-spaced pages (including graphs, drawings, photographs, and appendices) if it were to be printed on 8.5" x 11.0" paper, and the font should be no smaller than 10 pt. Times New Roman. Up to five of the 100 pages may be foldouts (11" x 17" max).

6. Design projects that are used as part of an organized classroom requirement are eligible and encouraged for competition.
7. The prizes shall be: First place-\$500; Second place-\$250; Third place-\$125 (US dollars). Certificates will be presented to the winning design team or individual for display at their university and a certificate will also be presented to each team member and the faculty/project advisor. One representative from the first place design team may be asked to present a summary paper at an AIAA Conference.

If a presentation is to be made, reasonable airfare and lodging will be defrayed by the AIAA Foundation for the team representative.

8. More than one design may be submitted from students at any one school, but only one design per team may be submitted.
9. If a design group withdraws their project from the competition, the team leader must notify AIAA Headquarters immediately.
10. Team competitions will be groups of not more than ten AIAA Student Members per entry. Individual competitions will consist of only 1 or 2 AIAA Student Member per entry.

## II. Copyright

All submissions to the competition shall be the original work of the team members.

Any submission that does not contain a copyright notice shall become the property of AIAA. A team desiring to maintain copyright ownership may so indicate on the signature page but nevertheless, by submitting a proposal, grants an irrevocable license to AIAA to copy, display, publish, and distribute the work and to use it for all of AIAA's current and future print and electronic uses (e.g. "Copyright © 20\_\_ by \_\_\_\_\_. Published by the American Institute of Aeronautics and Astronautics, Inc., with permission.).

Any submission purporting to limit or deny AIAA licensure (or copyright) will not be eligible for prizes.

## III. Schedule and Activity Sequences

Significant activities, dates, and addresses for submission of proposal and related materials are as follows:

- A. Letter of Intent — 31 January 2015
- B. Proposal delivered to AIAA Headquarters — 8 June 2015
- C. Announcement of Winners — August 2015

Groups intending to submit a proposal must submit a Letter of Intent (Item A), with a maximum length of one page to be received with the attached form on or before the date specified above. LOI must be emailed to Rachel Andino ([rachela@aiaa.org](mailto:rachela@aiaa.org)).

The email containing the finished proposal must be received at the same address on or

before the date specified above for the Receipt of Proposal (Item B).

## IV. Proposal Requirements

The technical proposal is the most important factor in the award of a contract. It should be specific and complete. While it is realized that all of the technical factors cannot be included in advance, the following should be included and keyed accordingly:

1. Demonstrate a thorough understanding of the Request for Proposal (RFP) requirements.
2. Describe the proposed technical approaches to comply with each of the requirements specified in the RFP, including phasing of tasks. Legibility, clarity, and completeness of the technical approach are primary factors in evaluation of the proposals.
3. Particular emphasis should be directed at identification of critical, technical problem areas. Descriptions, sketches, drawings, systems analysis, method of attack, and discussions of new techniques should be presented in sufficient detail to permit engineering evaluation of the proposal. Exceptions to proposed technical requirements should be identified and explained.
4. Include tradeoff studies performed to arrive at the final design.
5. Provide a description of automated design tools used to develop the design.



## V. Basis for Judging

### 1. *Technical Content (35 points)*

This concerns the correctness of theory, validity of reasoning used, apparent understanding and grasp of the subject, etc. are all major factors considered and a reasonably accurate evaluation of these factors presented?

### 2. *Organization and Presentation (20 points)*

The description of the design as an instrument of communication is a strong factor on judging. Organization of written design, clarity, and inclusion of pertinent information are major factors.

### 3. *Originality (20 points)*

The design proposal should avoid standard textbook information, and should show the independence of thinking or a fresh approach to the project. Does the method and treatment of the problem show imagination? Does the method show an adaptation or creation of automated design tools?

### 4. *Practical Application and Feasibility (25 points)*

The proposal should present conclusions or recommendations that are feasible and practical, and not merely lead the evaluators into further difficult or insolvable problems.

systems that are necessitated only or largely by the presence of a human pilot including displays, switches, g-seats, g-suits, oxygen, pressurization, and other environmental control systems. The aircraft's maneuver capabilities are limited by the pilot's physiological limits such as g tolerance, susceptibility to disorientation, or even physical endurance. With pilots onboard, all aspects of the aircraft design process are strongly impacted. The aircraft size, shape, and configuration arrangement are affected.

Providing adequate visibility leads to constrained forebodies and large canopies that increase the aircraft's drag signature. The design of the aircraft is strongly influenced by human-related issues such as safety factors, redundancy levels, failure modes, and vulnerability. Most of the useful life of today's combat aircraft is devoted to training and proficiency flying, thus requiring longer design lives than would be needed to meet combat requirements.

Removing the constraints imposed by the pilot could lead to revolutionary design approaches and should allow for dramatic new vehicle concepts. One class of vehicle that is of particular interest is Uninhabited Combat Air Vehicles (UCAV), of which this RFP is an example. The UCAV can be designed specifically for combat rather than primarily for proficiency flying. This would allow the vehicle to be optimized to do a specific mission and would enable it to complete radical new maneuvers impossible or even unimaginable with a pilot in the vehicle. The design approach for UCAVs would focus on designing a vehicle with a shorter operational life and with lower factors of safety and lower levels of redundancy than piloted aircraft. These new design approaches and aircraft concepts should provide dramatic improvements in performance such as reduced observables

## VI. Request for Proposal

### *Uninhabited Long Range Strike Vehicle*

#### 1.0 Background

Design provisions for the flight crew of combat aircraft place many constraints on the vehicle and its performance. Numerous cost and weight penalties are associated with



and drag and increased range, speed, payload, maneuverability, and survivability. These vehicles should be lighter, smaller, and less expensive than current or future piloted aircraft and as a consequence are a possible solution to an overwhelming issue for the military – the affordability of future weapon systems.

## **2.0 Statement of Objectives (Requirements)**

2.1 Design an uninhabited combat aerial vehicle (UCAV) to meet the requirements of the Uninhabited Long-Range Strike (ULRS) mission.

2.2 Attachment 1 provides specific information on the design mission.

2.3 Attachment 2 specifies minimum performance requirements.

## **3.0 Other Required Capabilities and Characteristics**

3.1 UCAV Control System (required): Aircraft will be semi-autonomous and controlled by a person in a ground control station (GCS) linked to the ULRS via satellite. The GCS will be similar to that currently used for the RQ-4 Global Hawk aircraft and decidedly different from the GCS used for the MQ-1 Predator and MQ-9 Reaper. The ULRS GCS will not be equipped for remotely hand-flying the aircraft as is done for MQ-1 and MQ-9. Rather, the operator will interact with ULRS through computer mission planning and monitoring touch screens.

3.2 Maintenance/Servicing (required): The design must allow easy access to and removal of primary elements of all major systems. Minimize requirements for unique support equipment—development of any new support equipment will be included in program cost estimates.

3.3 Structure (required): Design limit load factors are +12 and -8 vertical g's in the clean configuration at maximum gross weight. The structure should withstand a dynamic pressure of 2166 psf (Mach 1.2 at sea level). A factor of safety of 1.3 shall be used on all design ultimate loads. Primary structures should be designed for durability and damage tolerance. Design service life is 10,000 hours.

3.4 Fuel/Fuel Tanks (required): Primary design fuel is standard JP-8 or Jet-A (6.8 lb/gal = 50.87 lb/ft<sup>3</sup>) jet engine fuel. If external fuel tanks are required (this is not desirable) limit them to conformal fuel tanks that must be retained for the entire mission.

3.5 Stability (required): Unaugmented subsonic longitudinal static margin (S.M.) shall be no greater than 10% and no less than -5%. Maximum c.g. excursion for all loading conditions must not exceed 7% M.A.C. A digital flight control system is mandatory.

3.6 Cost: Costs requirements are broken into per unit production costs (recurring) and non-recurring (NRE) costs. Per unit production costs are defined as the average incremental cost for each aircraft and will include the entire aircraft. Due to learning curve and some production tooling costs, this cost may be affected to a small degree by the number of aircraft bought. NRE will consist of all development and production preparation costs. If unique support equipment is required, the cost of developing this equipment will be included in NRE. NRE costs will be considered fixed given no delays in the planned development program. When able, report both Development and Production NRE costs. Also, be prepared to report flyaway costs for a 200 aircraft buy. For initial estimates plan

on 10 flight test aircraft which may be included in the 200 aircraft buy.

- 3.6.1 Total NRE costs will not exceed \$10 billion in constant 2015 dollars
- 3.6.2 Per unit cost will not exceed \$200 million in constant 2014 dollars
- 3.6.3 All practical measures including reducing operations cost will be taken to minimize total life cycle costs.

#### 4.0 Measures Of Merit

Designs will be evaluated against design mission performance, other performance requirements, cost and the Measures of Merit described below. The following measures of merit will be reported:

4.1 Weight summary, gross takeoff weight, empty weight, mission fuel burn, wing loading ( $W_{TO}/S$ ), thrust-to-weight ratio ( $T_{SL}/W_{TO}$ ), mission fuel fraction ( $W_f/W_{TO}$ ) including external tanks, if used, and weight statements are required.

4.2 Aircraft geometry and systems integration (wing and control surface area, fuselage length, width/diameter, size and volume, frontal cross sectional area distribution, wetted area, inlet and diffuser, landing gear, sensor and avionics locations, crew station, etc.)

4.3 Mission duration, radius or range, fuel burn by mission segment for design mission.

4.4 Take-off and landing distance at max gross weight including standard day and icy runway balanced field length at sea level. For single-engine designs runway length requirements may be approximated by adding take-off and landing distance together. For multi-engine designs actual balanced field length should be considered.

4.5 Performance at combat weight (50% internal fuel) for ULRS design mission loadings.

4.5.1 Maximum Mach Number at 50,000 ft above mean sea level (MSL)

4.5.2 1-g Maximum Thrust Specific Excess Power Envelope

4.5.3 Time to accelerate from  $M = 0.93$  to  $M = 2.0$  at 50,000 ft MSL

4.5.4 Energy Maneuverability Diagram at 50,000 ft MSL

4.5.5 L/D vs Mach at 50,000 ft

4.6 NRE, per unit production cost, per unit flyaway cost, operations costs and total life cycle costs. Show cost trades for aircraft buys of 100 to 700 units.

4.7 A pictorial of a model of the aircraft is required. This may be a CAD model or photographs of a physical model.

4.8 Document a) concept selection trades and b) concept development trades.

4.9 Develop and present the alternative concepts considered leading to the downselect of your preferred concept. The methods and rationale used for the downselect shall be presented. At a minimum a qualitative assessment of strengths and weaknesses of the alternatives shall be given, discussing merits, leading to a justification as to why the preferred concept was the best proposal response. Quantitative justification of why the selected proposal is the best at meeting the proposal measures of merit(s) will strengthen the proposal.

4.10 Include the major trade studies conducted justifying the optimization, sizing, architectural arrangement and integration of the specifically selected proposal concept. Quantitative data shall be presented showing why your concept 'works' and is the preferred design compromise that best achieves the RFP requirements and objectives. Note that issues of observability are important considerations for aircraft of this

type; however, as the individual undergraduate aircraft design topic, students responding to this opportunity do not need to conduct analyses or studies of observability. Design concepts and studies that do use textbook-like approaches to address observability are welcome but these studies should not replace the focus on airframe design and performance as described above.

# Attachment 1

## High Altitude Supersonic Strike Mission

---

**Required configuration: (4) 1,000 lb JDAM**

Phase	Description
1	Fuel allowance for start (100 lb/engine), warm-up/taxi (50 lb/min/engine – plan on 30 minutes ground time), Mil power run up (200 lb/engine)
2	Take-off and acceleration allowance (computed at sea level. 59° F) <ol style="list-style-type: none"> <li>a. Fuel to accelerate to climb speed at take-off thrust (no distance credit)</li> </ol>
3	Climb from sea level to optimum supercruise altitude (Min fuel burn. Distance credit allowed.)
4	Supercruise out 800 nm total (including previous leg) at $M = 1.5$ and optimum altitude. Final cruise altitude must be above 50,000 ft.
5	Dash out 200 nm at $M = 2.0$ at or above 50,000 ft.
6	Zoom to less than $M = 0.93$ . Distance to zoom and ballistic range of weapon released at this altitude and Mach may be included in the 200 nm total range of the previous leg.
7	Weapons delivery: <p style="margin-left: 40px;">Fuel required to perform a single 180 degree turn at 50,000 ft or above and at least 0.85 Mach. If a descending turn is selected then remain above 50,000 ft for the entire maneuver.</p> <p style="margin-left: 40px;">Weapons delivery must be performed no faster than 0.93 Mach due to weapons limits.</p>
8	Accelerate to $M = 2.0$ . Remain above 50,000 ft.
9	Dash back 200 nm (including previous leg) at $M = 2.0$ at or above 50,000 ft.
10	Descend / climb to best cruise Mach and best cruise altitude (BCM/BCA).
11	Subsonic cruise back 800 nm at BCM/BCA.
12	Descend to sea level (No distance credit allowed).
13	Reserves: fuel for either 30 minutes or 10% of design mission time at 10,000 feet and speed for maximum endurance whichever is greater.

Note: Base all performance calculations on standard day conditions with no wind.



## Attachment 2

### ULRS Minimum Performance Requirements

---

<b>Criteria</b>	<b>Requirement</b>	<b>Actual</b>
Cruise Ceiling	60,000 ft	
Runway Length	10,000 ft	
Payload (expendable)	4,100 lb	
Range (unrefueled)	2,000 nm at M = 1.6	
Cruise Mach	1.5	
Dash Mach	2.0	
Time to Accelerate for M = 0.93 to M = 2.0 at 50,000 ft	2 minutes maximum	
NRE	\$10 billion	
Flyaway Cost	\$200 Million for 200-aircraft buy. Show cost trades for 100 to 700 aircraft	

## **Appendix B: QF-36 Concept Design Drawings**

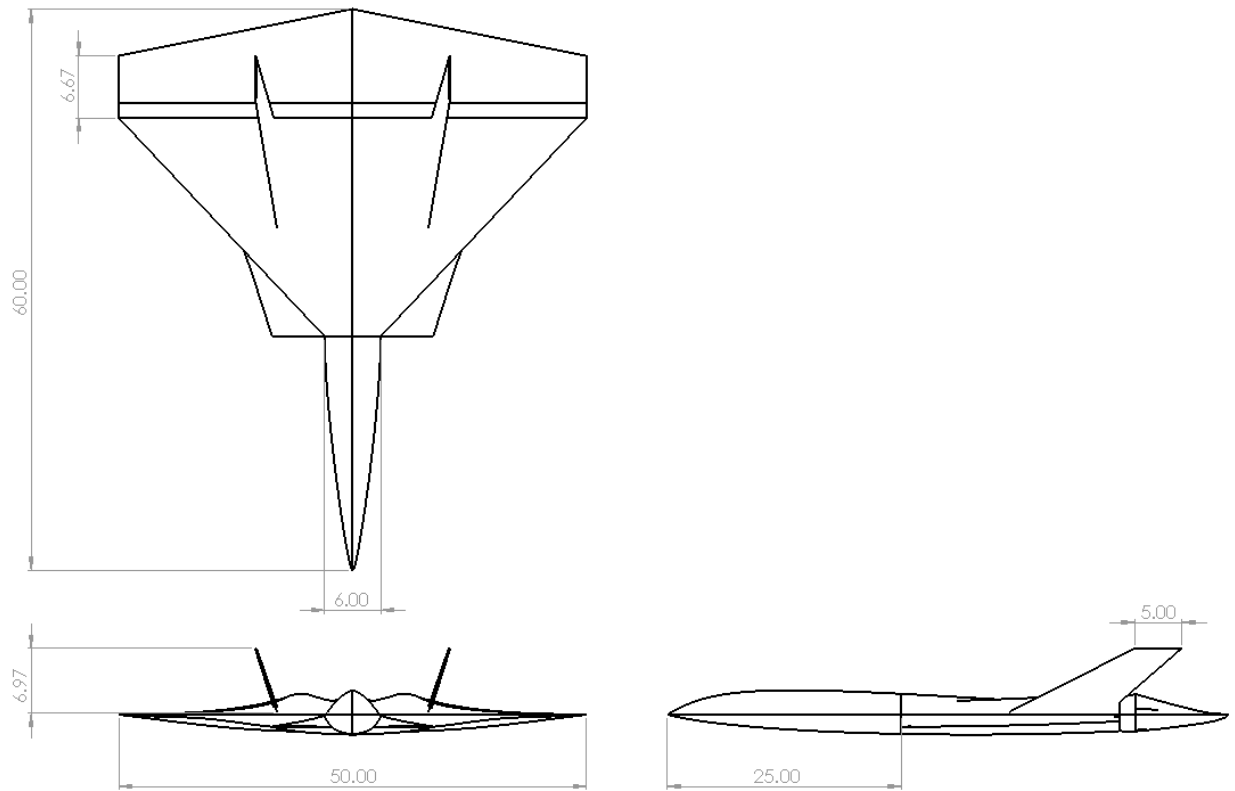


**Figure B 1: Three-view drawing of UCAV QF-36 with dimensions.**

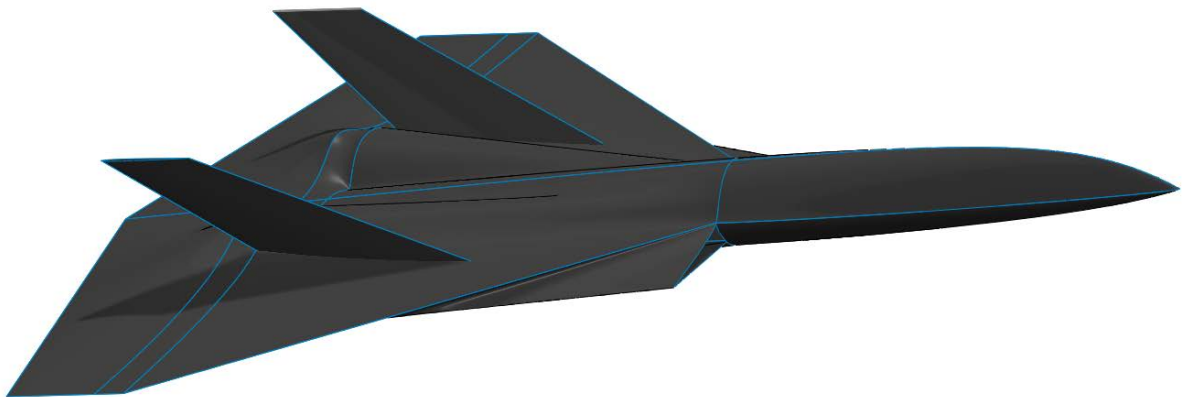


**Figure B2: UCAV QF-36, view 1.**

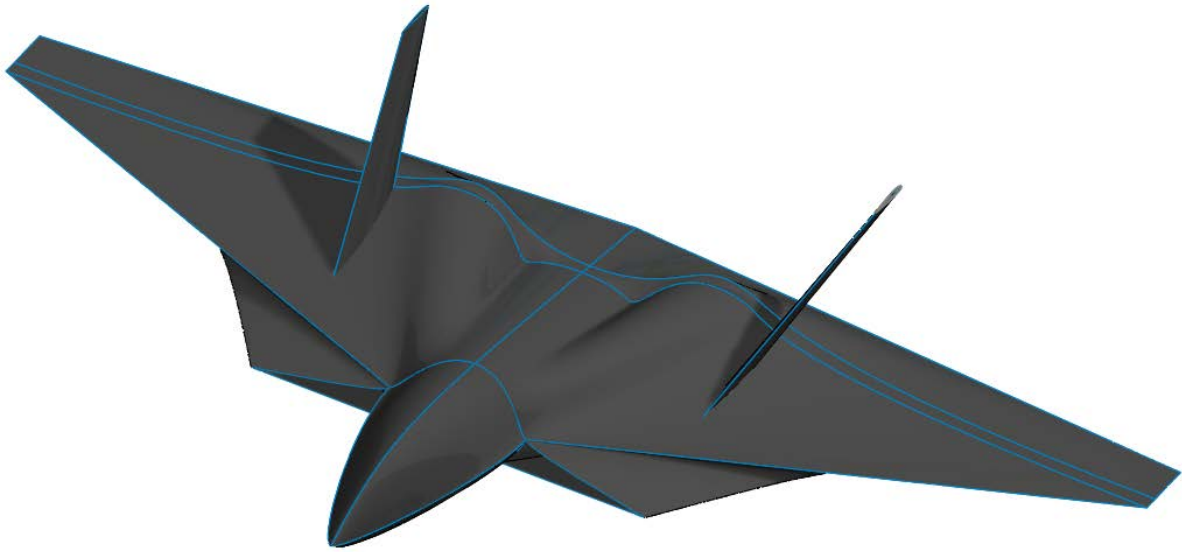


**Figure B3: UCAV QF-36, view 2.**

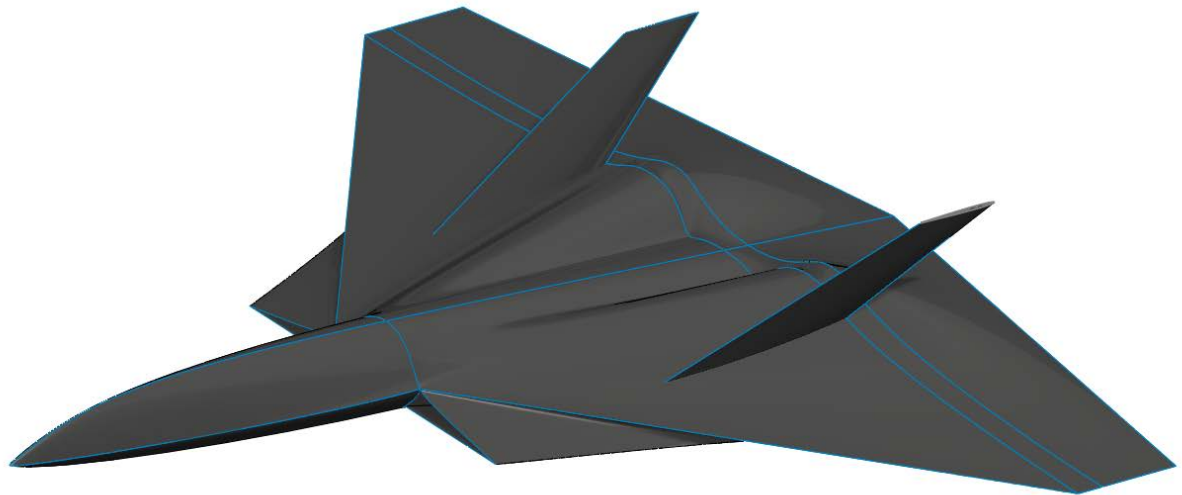


**Figure B4: UCAV QF-36, view 3.**



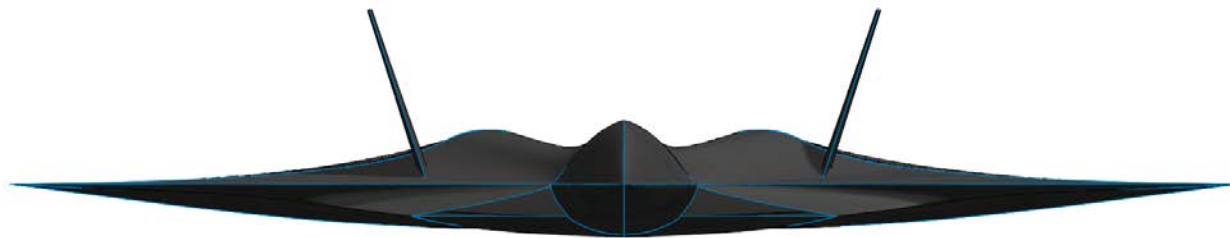


**Figure B 5: UCAV QF-36, front-view.**

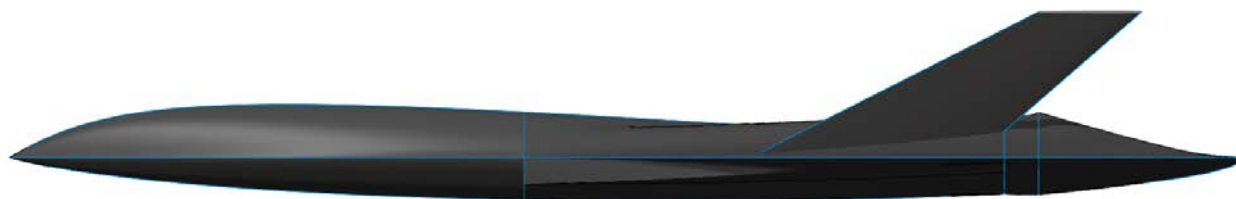


**Figure B 6: UCAV QF-36, side-view.**

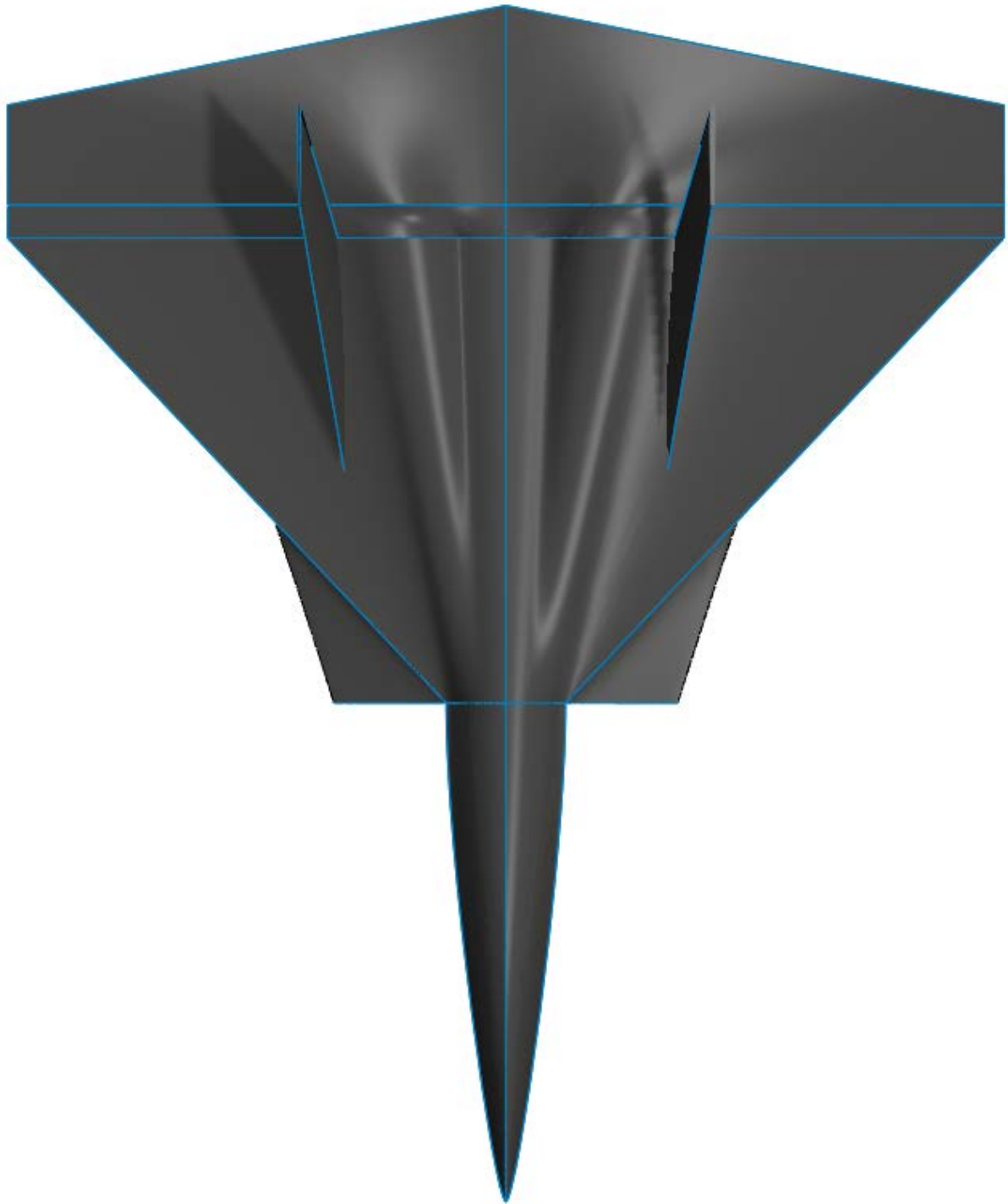


**Figure B 7: UCAV QF-36, top view.**